Zero-Shot Unsupervised and Text-Based Audio Editing Using DDPM Inversion

Hila Manor [1] **Tomer Michaeli** [1]

Abstract

Editing signals using large pre-trained models, in a zero-shot manner, has recently seen rapid advancements in the image domain. However, this wave has yet to reach the audio domain. In this paper, we explore two zero-shot editing techniques for audio signals, which use DDPM inversion on pre-trained diffusion models. The first, adopted from the image domain, allows text-based editing. The second, is a novel approach for discovering semantically meaningful editing directions without supervision. When applied to music signals, this method exposes a range of musically interesting modifications, from controlling the participation of specific instruments to improvisations on the melody. Samples can be found on our examples page. Code can be found here.

1. Introduction

Creative media creation has seen a dramatic transformation with the recent advancements in text-based generative models, particularly those based on denoising diffusion models (DDMs) (Sohl-Dickstein et al., 2015; Ho et al., 2020; Song et al., 2020). While progress has been initially made in image synthesis (Ramesh et al., 2021; Rombach et al., 2022), generative models for the audio domain have recently captured increased interest. Indeed, transformer based models such as MusicGen (Copet et al., 2023) and MusicLM (Agostinelli et al., 2023), and diffusion based models such as AudioLDM (Liu et al., 2023a) and TANGO (Ghosal et al., 2023), now enable nonprofessional users to effortlessly create short musical excerpts and audio effects.

To allow more fine-grained manipulations, a lot of attention has been recently devoted to *editing* of signals using DDMs. In the image domain, some works proposed to train from scratch text-guided models for editing (Brooks et al., 2023), or to use test-time optimization to control the generation or to fine-tune a pre-trained text-to-image model (Gal et al., 2022; Kim et al., 2022; Kawar et al., 2023; Ruiz et al., 2023; Zhang et al., 2023b). Other works demonstrated that high quality results can be obtained with zero-shot editing methods that employ pre-trained text-to-image models (Meng et al., 2021; Huberman-Spiegelglas et al., 2023; Tumanyan et al., 2023; Wu & De la Torre, 2023), avoiding the heavy computational burden of test-time optimization. In the audio domain, text-based editing has only very recently started gaining traction. Recent works either train models from scratch for specific editing tasks (Copet et al., 2023; Han et al., 2023; Wang et al., 2023), or apply test-time optimization (Paissan et al., 2023; Plitsis et al., 2023). To date, zero-shot editing for audio signals has only been illustrated in the AudioLDM work (Liu et al., 2023a), using the naive SDEdit (Meng et al., 2021) approach.

In this paper we explore two approaches for zero-shot audio editing with pre-trained audio DDMs, one based on *text guidance* and the other based on semantic perturbations that are found in an *unsupervised* manner. Our text-guided editing technique allows a wide range of manipulations, from changing the style or genre of a musical piece to changing specific instruments in the arrangement (Fig. 1(c),(d)), all while maintaining high perceptual quality and semantic similarity to the source signal. Our unsupervised technique allows generating *e.g.*, interesting variations in melody that adhere to the original key, rhythm, and style, but are impossible to achieve through text guidance (Fig. 1(a),(b)).

Our methods are based on the recently introduced edit-friendly DDPM inversion method (Huberman-Spiegelglas et al., 2023), which we use for extracting latent noise vectors corresponding to the source signal. To generate the edited signal, we use those noise vectors in a DDPM sampling process (Ho et al., 2020), while drifting the diffusion towards the desired edit. In text-based editing, we achieve this by changing the text prompt supplied to the denoiser model. In our unsupervised method, we perturb the output of the denoiser in the directions of the top principal components (PCs) of the posterior, which we efficiently compute based on Manor & Michaeli (2024). As we show, these perturbations are particularly useful for editing music excerpts, in which they can uncover improvisations and other musically plausible modifications.

We compare our methods to the state-of-the-art text-to-music model MusicGen (Copet et al., 2023), whose genera-

[1]Technion – Israel Institute of Technology, Haifa, Israel. Correspondence to: Hila Manor <hila.manor@campus.technion.ac.il>.

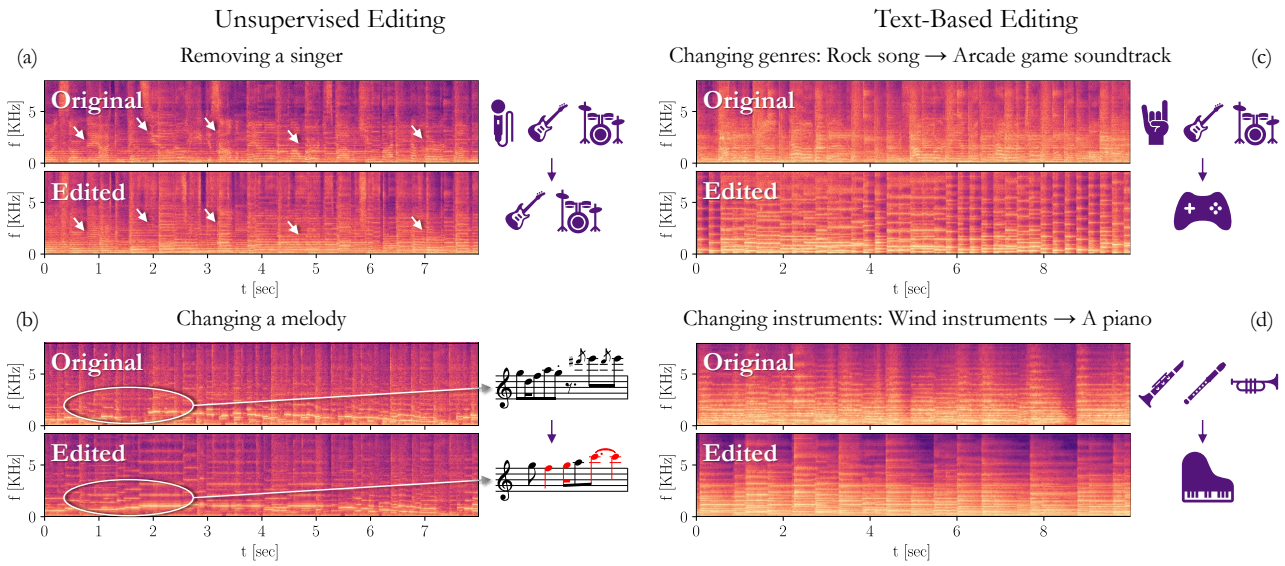

Figure 1. **Zero-shot audio editing.** We present two methods for editing audio signals using DDMs, a novel unsupervised approach (left), and a text-based approach adopted from the image domain(right). Both methods can edit a variety of concepts from style to instrumentation. (a) The singer (curved pitches) is removed while the rest of the signal remains intact. (b) The melody notes change, reflected by a change in the dominant pitch. (c) The genre is changed, affecting the entire statistics of the spectrogram. (d) The instrumentation changes from a woodwind section to a piano, visible by the attack (abrupt starts) of the piano keys. All examples can be listened to in our examples page. For (c),(d), $T_{\text{start}} = 100, 130$, respectively (Sec. 3.2). For (a),(b), $T_{\text{start}} = 150, 200$, $t' = 115, 80$, $T_{\text{end}} = 1$, using the top 3 PCs (Sec. 3.3).

tion process can be conditioned on a given music piece, as well as to using the zero-shot editing methods SDEdit (Meng et al., 2021) and DDIM inversion (Song et al., 2021; Dhariwal & Nichol, 2021) in conjuction with the AudioLDM model (Liu et al., 2023a). We show that our approaches outperforms these methods in terms of generating semantically meaningful modifications, while remaining faithful to the original signal's structure.

2. Related Work

Specialized audio editing models. The most common approach for editing audio is to train specialized models for this particular task. MusicGen (Copet et al., 2023) and MusicLM (Agostinelli et al., 2023) train language based models for generating audio conditioned on text, and optionally also on a given melody. Editing a music excerpt with MusicGen is achieved by conditioning the generation on the excerpt's chromagram while supplying a text prompt describing the desired edit. However, because of its reliance on chromagrams, it typically fails in editing polyphonic music. MusicLM conditioning is built on a novel proprietary joint music-text embedding space, named MuLan, built to encode monophonic melodies. A different approach, borrowed from the image domain (Brooks et al., 2023), is to train an instruction based diffusion model for editing. This has been done for general audio (Wang et al., 2023) as well as specifically for music (Han et al., 2023). These methods are limited to a small set of modifications (*e.g.*, "Add", "Remove", "Replace") and require training on a large dataset of triplets (text prompt, input audio, and output audio). Our methods require no training and are not limited to a fixed set of instructions.

Test-time optimization. Instead of training a model from scratch, some works leverage large pre-trained models for editing. Paissan et al. (2023) and Plitsis et al. (2023) demonstrated the effectiveness of test-time optimization methods, adopted from the image domain (Gal et al., 2022; Kawar et al., 2023; Ruiz et al., 2023), to editing of audio signals. These methods either fine-tune the diffusion model to reconstruct the given signal (Ruiz et al., 2023), optimize the text-embedding to reconstruct the signal (Gal et al., 2022), or do both (Kawar et al., 2023). However, optimizing a new model for each signal is computationally intensive. Moreover, these methods struggle with changing specific concepts, *e.g.*, replacing only the piano in a music piece with a banjo. Our techniques avoid test-time optimization, and can achieve focused edits.

Zero-shot editing. Some works focus on zero-shot editing using pre-trained diffusion models. Perhaps the simplest approach is SDEdit (Meng et al., 2021), which adds noise to the signal and then runs it through the reverse diffusion process with a different text prompt. SDEdit was recently used for audio (Liu et al., 2023a) as well as for piano-roll

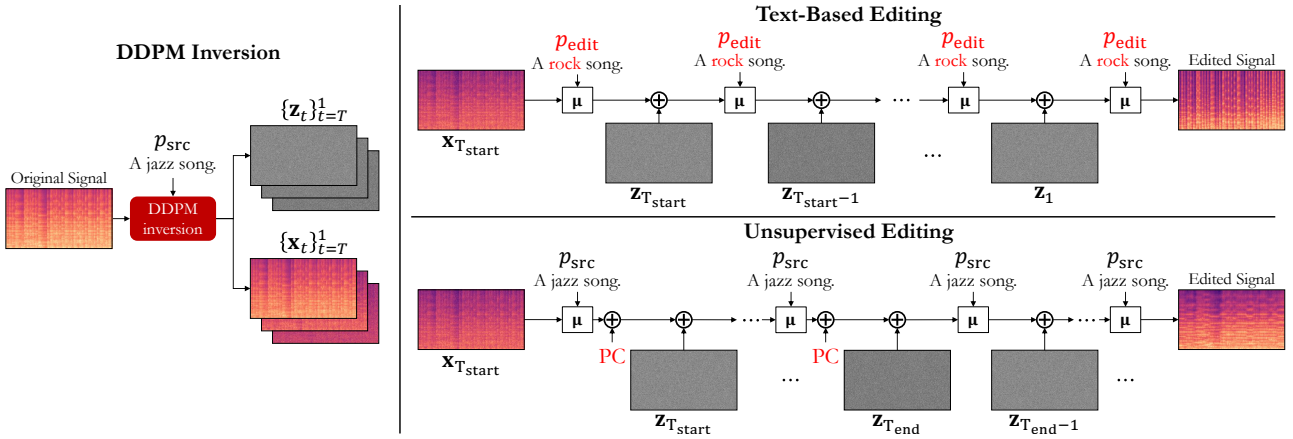

Figure 2. **Overview of our text-based and unsupervised editing methods.** We start by extracting the noise vectors corresponding to an input signal using DDPM inversion, optionally conditioned on a text prompt p_{src}. For the text-based editing approach, we then continue the reverse process with a different text prompt. For the unsupervised approach, we continue the reverse process when applying PCs calculated on the forward process. Red color shows what changed in the reverse process.

music (Zhang et al., 2023a). However it suffers from a severe tradeoff between adherence to the text and adherence to the original signal. Another direction, which has become popular in the image domain, is to use inversion techniques that extract the diffusion noise vectors corresponding to the source signal. One method for doing so is DDIM inversion (Song et al., 2021; Dhariwal & Nichol, 2021). This method was found suboptimal for editing images on its own, and is therefore typically accompanied by intervention in the attention maps during the diffusion process (Hertz et al., 2022; Cao et al., 2023; Tumanyan et al., 2023). Another approach is DDPM inversion (Huberman-Spiegelglas et al., 2023; Wu & De la Torre, 2023), which is conceptually similar, but applies to the DDPM sampling scheme. Here we adopt the DDPM inversion method of Huberman-Spiegelglas et al. (2023), which has shown state-of-the-art results in the image domain.

Unsupervised editing. Finding semantic editing directions in an unsupervised manner, without any guidance or reference samples, has been exhaustively studied in the context of GANs (Spingarn et al., 2020; Shen et al., 2020; Shen & Zhou, 2021; Wu et al., 2021). Recently, several works proposed ways for finding editing directions in the bottleneck features (h-space) (Kwon et al., 2022) of a diffusion model (Haas et al., 2023; Park et al., 2023; Jeong et al., 2024) in an unsupervised manner. The unsupervised method we explore in this paper finds editing directions in the noise space of the diffusion model. This is done through adaptation of the method of Manor & Michaeli (2024), which quantifies uncertainty in Gaussian denoising.

3. Method

3.1. DDPM Inversion

Denoising diffusion probabilistic models (DDPMs) (Ho et al., 2020) generate samples through an iterative process, which starts with a Gaussian noise vector $\mathbf{x}_T \sim \mathcal{N}(0, \boldsymbol{I})$ and gradually denoises it in T steps as

$$\mathbf{x}_{t-1} = \boldsymbol{\mu}_t(\mathbf{x}_t) + \sigma_t \mathbf{z}_t, \quad t = T, \ldots, 1. \tag{1}$$

Here, $\{\mathbf{z}_t\}$ are iid standard Gaussian vectors, $\{\sigma_t\}$ is an increasing sequence of noise levels, and $\boldsymbol{\mu}_t(\mathbf{x}_t)$ is a linear function of $\hat{\mathbf{x}}_{0|t}$, which is the MSE-optimal prediction of a clean signal $\mathbf{x}_0$ from its noisy version

$$\mathbf{x}_t = \sqrt{\bar{\alpha}_t}\mathbf{x}_0 + \sqrt{1-\bar{\alpha}_t}\boldsymbol{\epsilon}_t, \quad \boldsymbol{\epsilon}_t \sim \mathcal{N}(0, \boldsymbol{I}). \tag{2}$$

The coefficients $\{\bar{\alpha}_t\}$ monotonically decrease from 1 to 0.

Rather than generating a synthetic signal, here we are interested in editing a real audio excerpt, $\mathbf{x}_0$. To do so, we follow the general approach of Huberman-Spiegelglas et al. (2023) and Wu & De la Torre (2023). Specifically, we start by extracting noise vectors $\{\mathbf{x}_T, \mathbf{z}_T, ..., \mathbf{z}_1\}$ that cause the sampling process (1) to generate the given signal $\mathbf{x}_0$ at $t = 0$. This is called *inversion*. We then use those noise vectors to sample a signal using (1) while steering the generation towards a desired edit effect, as we detail in Sections 3.2 and 3.3. To extract the noise vectors, we use the edit-friendly DDPM inversion method of Huberman-Spiegelglas et al. (2023). This method accepts as input the source signal $\mathbf{x}_0$ and generates from it an auxiliary sequence of vectors

$$\mathbf{x}_t = \sqrt{\bar{\alpha}_t}\mathbf{x}_0 + \sqrt{1-\bar{\alpha}_t}\tilde{\boldsymbol{\epsilon}}_t, \quad t = 1, \ldots, T, \tag{3}$$

where $\tilde{\boldsymbol{\epsilon}}_t$ are sampled independently from $\mathcal{N}(0, \boldsymbol{I})$. It then extracts the noise vectors by isolating them from (1) as

$$\mathbf{z}_t = (\mathbf{x}_{t-1} - \boldsymbol{\mu}_t(\mathbf{x}_t))/\sigma_t, \quad t = T, \ldots, 1. \tag{4}$$

While the noise vectors constructed this way have a different distribution than those participating in the original generative process (1), they have been shown to encode the global structure of the signal $\mathbf{x}_0$ more strongly, making them particularly suitable for editing tasks.

We note that a diffusion process can be either performed in the raw waveform space or in some latent space (Rombach et al., 2022). In this work we utilize the pre-trained AudioLDM2 (Liu et al., 2023a;b) model, which works in a latent space. AudioLDM2 generates mel-spectograms conditioned on text. Those mel-spectograms are decoded into waveforms using HiFi-GAN (Kong et al., 2020).

3.2. Text-Based Editing

The first editing approach we consider uses text guidance. In this setting, our goal is to edit a real audio signal $\mathbf{x}_0$ by using a text prompt p_{edit} describing the desired result. Optionally, a user may also want to describe the original signal with some text prompt, p_{src}, so as to achieve a more fine-grained modification.

To achieve this goal, we adopt the method of Huberman-Spiegelglas et al. (2023), which has been only explored in the image domain. Specifically, we start by inverting the signal $\mathbf{x}_0$ using (3),(4). We do this while injecting to the denoiser network the prompt describing the source, p_{src}. This is illustrated in the left pane of Fig. 2. We then run the generative process (1) with the extracted noise vectors, while injecting the prompt p_{edit} describing the desired output (top-right pane of Fig. 2). In both directions, we use classifier-free guidance (Ho & Salimans, 2021) for the text guidance. The noise vectors extracted from the source signal ensure that the generated signal has the same "coarse structure" as the source, while the change in the text conditioning affects more fine-grained features, and leads to the editing effect.

The balance between adhering to the target text and remaining loyal to the original signal can be controlled using two parameters. The first is the strength factor of the classifier free guidance. Increasing this parameter steers the generation more strongly towards the desired text at the expense of departing from the original signal. The second parameter is the timestep T_{start} from which we begin the generation process. This timestep can generally be smaller than T, and the smaller it is, the more the edited signal remains consistent with the source signal (see Sec. 4.3 for examples). We note that editing can be confined to a user-chosen segment, rather than applied to the whole signal (see App. B).

3.3. Unsupervised Editing

Editing using text guidance is limited by the expressiveness of the text prompt and by the model's language understanding. This is arguably very significant in music, where a user may want to generate *e.g.*, variations, improvisations, or modifications to the arrangement of the piece, which are virtually impossible to precisely describe by text. To support these kinds of edits, here we pursuit a different approach, which extracts in an unsupervised manner semantically meaningful editing directions in the noise space of the diffusion model. As we show, these directions can be used to perturb the generation process in multiple ways, enabling controllable semantic modifications to the signal.

As in Sec. 3.2, we start by performing edit-friendly DDPM inversion to extract noise vectors corresponding to $\mathbf{x}_0$, optionally using a text-prompt describing the signal, p_{src}. We then use those vectors in the sampling process (1), but with perturbations. Specifically, recall from Sec. 3.1 that each timestep t involves $\hat{\mathbf{x}}_{0|t}$, the MSE-optimal prediction of $\mathbf{x}_0$ from $\mathbf{x}_t$. This prediction, obtained from the denoiser, corresponds to the posterior mean $\mathbb{E}[\mathbf{x}_0|\mathbf{x}_t]$. Our approach is to perturb this posterior mean along the top principal components (PCs) of the posterior, *i.e.*, the top eigenvectors of the posterior covariance $\mathrm{Cov}[\mathbf{x}_0|\mathbf{x}_t]$. This approach has been recently studied in the context of uncertainty visualization in inverse problems (Nehme et al., 2023; Manor & Michaeli, 2024), where it was illustrated to nicely reveal the dominant modes of uncertainty about the MSE-optimal prediction.

To compute the posterior PCs, we use the method of Manor & Michaeli (2024). This work showed that the posterior covariance in Gaussian denoising is proportional to the Jacobian of the MSE-optimal denoiser. It further showed that extracting the top eigenvectors and eigenvalues of this Jacobian can be done using the subspace iteration method (Saad, 2011), where each iteration can be approximated using a single forward pass through the denoiser network. See App. C for a detailed algorithm.

Having computed the posterior PCs $\{\mathbf{v}_{i|t'}\}$ and their corresponding eigenvectors $\{\lambda_{i|t'}\}$ at some timestep t', we can add or subtract each of them to the denoised signal $\hat{\mathbf{x}}_{0|t}$ at every timestep $t \in [T_{\text{start}}, \ldots, T_{\text{end}}]$ using a matching factor $\gamma\lambda_{i|t}^{1/2}$, where γ is a user-chosen parameter controlling the strength of the modification. As we show in App. C, adding the vector $\gamma\lambda_{i|t}^{1/2}\mathbf{v}_{i|t'}$ to $\hat{\mathbf{x}}_{0|t}$, is equivalent to adding it to $\boldsymbol{\mu}_t(\mathbf{x}_t)$ from Eq. (1) with a correction factor. Specifically, this modifies the generation process into

$$\mathbf{x}_{t-1} = \boldsymbol{\mu}_t(\mathbf{x}_t) + \gamma c_t \lambda_{i|t}^{1/2}\mathbf{v}_{i|t'} + \sigma_t \mathbf{z}_t, \quad t = T, \ldots, 1. \tag{5}$$

where $c_t = \sqrt{\bar{\alpha}_{t-1}} - \sqrt{\bar{\alpha}_t}\sqrt{1-\bar{\alpha}_{t-1}-\sigma_t^2}/\sqrt{1-\bar{\alpha}_t}$. Note that instead of adding a single PC, $\mathbf{v}_{i|t'}$, we can add a linear combination of PCs, thereby creating a new direction that changes multiple semantic elements at once.

The addition of PCs can be done in two different ways. The first is to use $t' = t$ in (5), so that each denoising step is perturbed with its own PCs. The second way involves

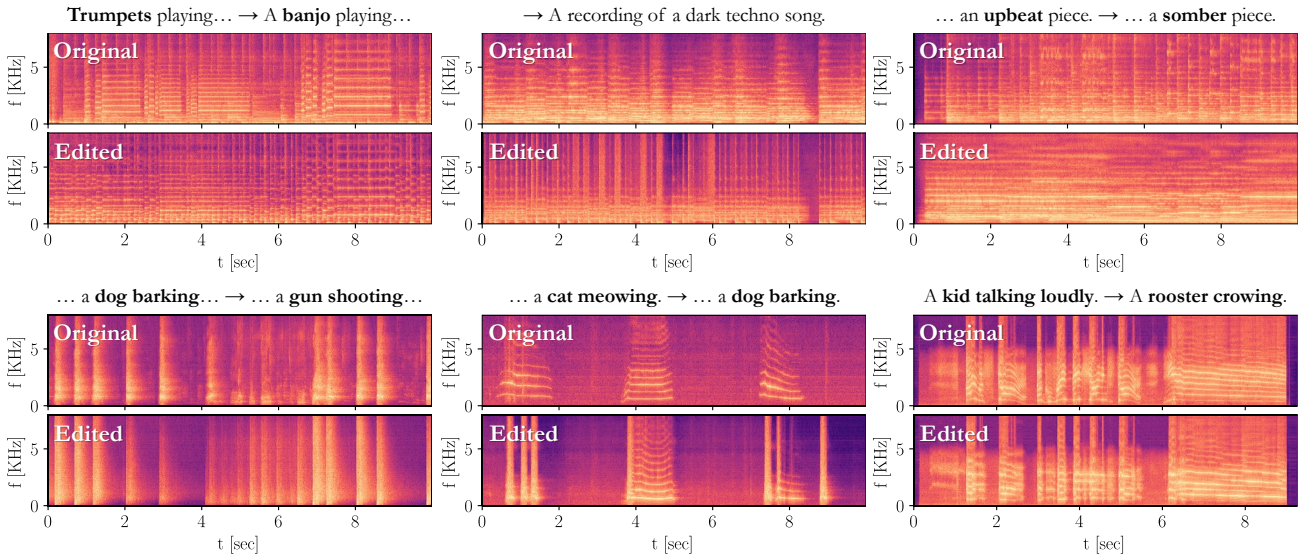

Figure 3. **Text-based zero-shot editing.** Text-based editing enables changing a plethora of elements in a signal, from the genre of a song, to the objects heard in a recording. All examples can be listened to in Sec. 1.1.1 of our examples page. The source and target text prompts are shown above the spectrograms, where bold marks changed text. The parameter T_{start} (Sec. 3.2), from top to bottom and left to right, is 110, 110, 120, 100, 50, 90. The first line used the music checkpoint of AudioLDM2, while the second used the large general checkpoint.

extracting a direction from some specific timestep t', and adding it at all timesteps $t \in [T_{\text{start}}, \ldots, T_{\text{end}}]$, where t' need not necessarily be a member of this set. In this case, it is important to use the factor $\lambda_{i|t}$ that matches the timestep t to which the perturbation is added, and not the factor $\lambda_{i|t'}$ corresponding to the timestep at which the PC was computed. The role of this factor is to match the applied change to the uncertainty level at the current timestep.

Adding the same direction at all timesteps usually strongly modifies a specific element, *e.g.*, a single note or the strength of a vibrato effect. Adding to each timestep its own PC can lead to a larger deviation from the original signal, *e.g.*, emphasizing a singer or changing a melody. This is because the extracted PCs can wildly differ in semantics and locality across a large range of timesteps.

We empirically find that for each PC index i, the values of $\{\lambda_{i|t}\}_{t=1}^{T}$ are similar across signals and AudioLDM2 checkpoints. We therefore compute their average value over a dataset once, and use these average values for all signals.

4. Experiments

To evaluate our editing methods we used AudioLDM2 (Liu et al., 2023b) as the pre-trained model, using 200 inference steps as recommended by the authors. In our text-based editing experiments we compare to MusicGen (Copet et al., 2023) conditioned on melody using their medium checkpoint, and to DDIM inversion (Song et al., 2021; Dhariwal & Nichol, 2021) and SDEdit (Meng et al., 2021) using the same AudioLDM2 checkpoint as we use. To evaluate our unsupervised editing method, we compare it to SDEdit, where we supply it with a prompt describing the source signal (rather than the desired edited signal). This baseline performs uncontrolled modifications to the signal, whose strength we choose using the starting timestep.

We do not compare to AUDIT (Wang et al., 2023) and InstructME (Han et al., 2023), which train a model specifically for editing purposes, as they did not share their code and trained checkpoints. Additionally, we do not compare to DreamBooth and Textual Inversion as demonstrated on audio by Plitsis et al. (2023), since they solve a different task – that of personalization. This task aims at learning a concept from a reference audio, rather than consistently modifying the input itself. Thus, personalization may allow *e.g.*, changing a genre, but cannot be used for fine-grained edits such as changing a specific instrument into a different one. In fact, as Plitsis et al. (2023) show, both methods have difficulty preserving the key and dynamics of the original piece, where textual inversion fails to even retain the same tempo. We encourage the reader to listen to our results and qualitative comparisons on our examples page.

4.1. Datasets

To enable a systematic analysis and quantitative comparison to other editing methods, we use the MusicDelta subset of the MedleyDB dataset (Bittner et al., 2014), comprised of 34 musical excerpts in varying styles and in lengths ranging from 20 seconds to 5 minutes, and create and re-

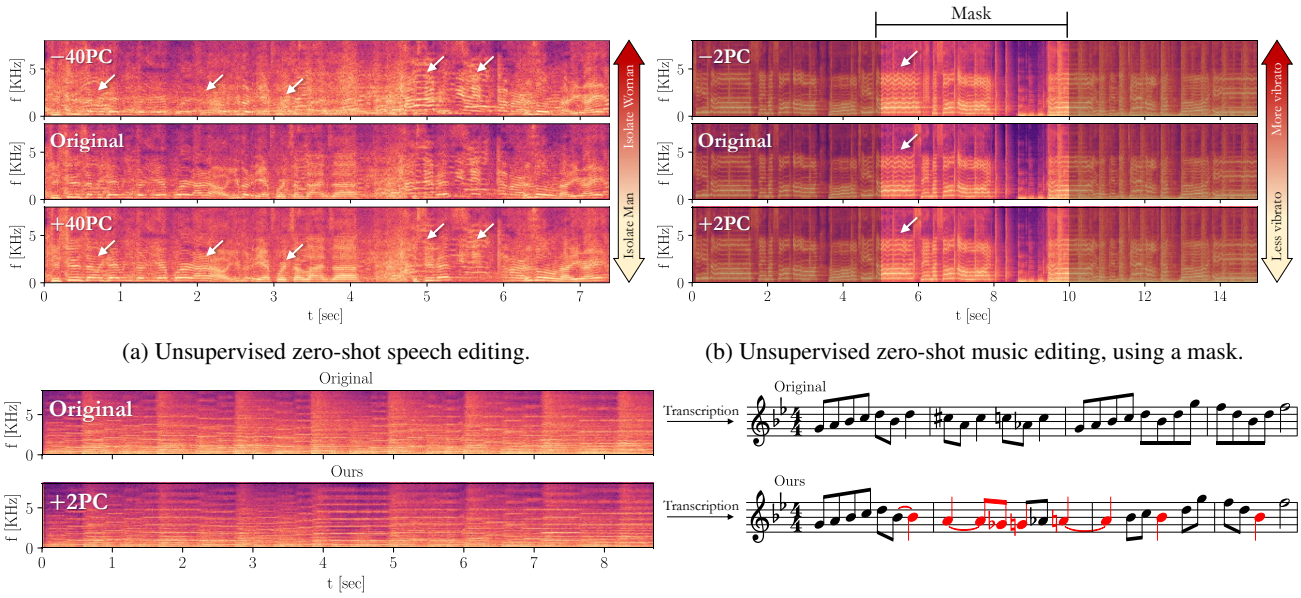

(a) Unsupervised zero-shot speech editing.

(b) Unsupervised zero-shot music editing, using a mask.

(c) Unsupervised melody improvisation.

Figure 4. **Unsupervised zero-shot editing.** Our unsupervised editing directions carry semantic meanings, ranging from separation of the persons in a conversation (a) to the vibrato of a singer (b) or a change in melody (c), all while retaining high semantic similarity to the source. Directions can be easily calculated and applied on a segment of the signal using a mask (c) (see App. B). All examples can be listened to in Sec. 1.2 of our examples page. In (a) we use $t' = t$, $T_{\text{start}} = 115$, $T_{\text{end}} = 95$, in (b) we fix $t' = 120$ and use $T_{\text{start}} = 150$, $T_{\text{end}} = 1$, and in (c) $t' = 95$, $T_{\text{start}} = 150$, $T_{\text{end}} = 50$. The PCs shown are the 1^{st} ,3^{rd}, and a combination of the first 3 PCs, respectively. The speech example uses the large checkpoint of AudioLDM2, without a source prompt, and the rest use the music checkpoint, with a source prompt randomly chosen from our prompts dataset.

lease with our code base a corresponding small dataset of prompts. This prompts dataset includes 3-4 source prompts for each signal, and 3-12 editing target prompts for each of the source prompts, totalling 107 source prompts and 696 target prompts, all labeled manually by the authors. We design the prompts to complement each other, *e.g.*, if the source prompts mentions a saxophone is playing, its target prompts may swap only the word "saxophone" with "guitar" or "piano". We additionally design some of the target prompts such that they do not require a complementary source prompt, and should provide enough information to edit a signal on their own (*e.g.*, for genre change). In our supervised text-guided experiments we randomly sub-sample a third of the source-target prompts pairs for each signal (where we include additional pairs with an empty source prompt where applicable). Thus, we evaluate our supervised prompt-based method on 324 signal-text pairs. In our unsupervised uncertainty-based experiments we randomly sub-sample one of the source-prompts per audio signal.

We remark that some works use MusicCaps (Agostinelli et al., 2023) to quantitatively evaluate synthesized samples. However, this dataset contains only 10-second long music excerpts, while real music pieces can vary wildly over longer segments, changing instruments, genre or key completely. This aspect is important in the context of text-based editing, where the signal may be a minute long, and the edit should remain consistent across the entire piece (*e.g.*, when changing one instrument into another).

4.2. Metrics

We quantitatively evaluate the results using three types of metrics; a CLAP (Wu et al., 2023; Chen et al., 2022) based score to measure the adherence of the result to the target-prompt (higher is better); LPAPS (Iashin & Rahtu, 2021; Paissan et al., 2023), an audio LPIPS (Zhang et al., 2018) measure to quantify the consistency of the edited audio relative to the source audio (lower is better); and FAD (Kilgour et al., 2018), an audio FID (Heusel et al., 2017) metric to measure the distance between two distributions of audio signals. FAD has been used in the past with deep features of VGGish (Hershey et al., 2017) or other convolutional neural networks (CNNs) trained on VGGSound (Chen et al., 2020). However, Gui et al. (2024) have shown that using such methods as a perceptual metric for music signals is sub-optimal, and so we follow their suggestion by using instead a trained large CLAP model (Wu et al., 2023) for the deep features of the FAD calculation. LPAPS has also been used in the past using CNNs trained on VGGSound, nevertheless

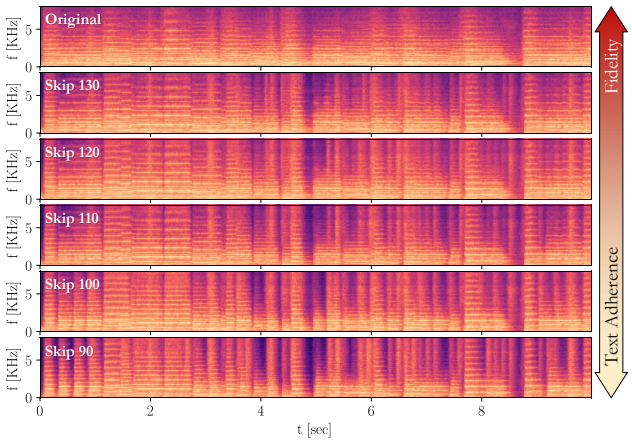

Figure 5. **The effect of T_{start} in text-based editing.** Here, an orchestral piece is edited by using only a target prompt, p_{edit}="A recording of a funky jazz song.". The signal retains more elements of the original signal as editing starts at a later timestep, denoted by T_{start}. This comes at a cost of adherence to the desired text description, *e.g.*, less coherent beats as expected by a funky jazz song, and more elongated notes as in the original orchestral piece. This example can be listened to in Sec. 1.1.2 of our examples page.

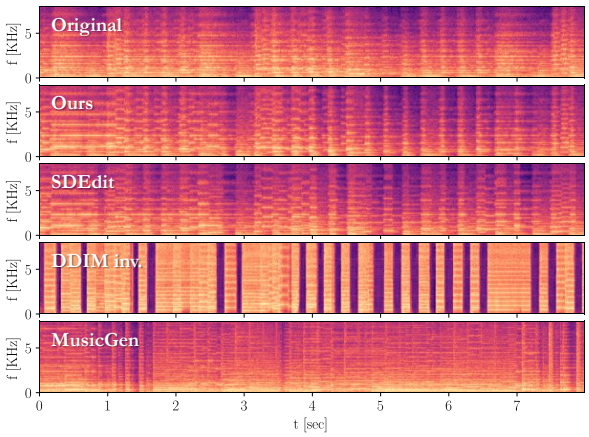

Figure 6. **Comparison of methods for text-based editing.** We compare our method, SDEdit (Meng et al., 2021), DDIM Inversion, and MusicGen (Copet et al., 2023) for editing of the same signal. All of the results achieve a CLAP score of~ 0.34, however the LPAPS values are $4.29, 4.87, 6.26, 5.74$, respectively. This means that our method is most loyal to the original structure. Here for our method we use $T_{\text{start}} = 120$ and for SDEdit $T_{\text{start}} = 130$.

we continue with the same reasoning and use intermediate features from the same CLAP model as LPAPS' backbone in our evaluations. In particular, we use the output layers of the four intermediate Swin-transformer blocks (Liu et al., 2021) of the CLAP model as LPAPS' features. More details can be found in App. A.

4.3. Text-Based Editing

Results for different effects achieved with our text-based editing method are shown in Fig. 1(c),(d) and Fig. 3. In this setting we set the classifier-free guidance strength of the target prompt to 12 for SDEdit and for our method, and to 5 for DDIM inversion. The classifier-free guidance strength for the source prompt is set to 3. Text-based editing allows changing the global semantics of the signal, *e.g.*, by changing one instrument to another or by changing the genre of the song. All examples and more can be listened to in Sec. 1.1.1 of our examples page.

Fig. 5 shows the effect of T_{start}. This parameter controls the trade-off between the adherence of the edited signal to the target prompt p_{edit}, and its fidelity to the original signal. This effect can also be listened to in Sec. 1.1.2 of our webpage.

To quantitatively measure the adherence of the edited signals to the target prompt and their fidelity to the source excerpts, we plot the CLAP-LPAPS results for all methods in Fig. 8. For SDEdit and for our method we plot results for multiple T_{start} values. It is evident that MusicGen, which is trained to be conditioned on a chromagram of the input signal, does not enable transferring a concept in the same way as the zero-shot editing methods we explore. As can be seen, our method outperforms all other methods under any desired balance between fidelity and text-adherence. Qualitative comparisons can be listened to in Sec. 2.1 of our examples page. Figure 6 includes a visual comparison.

4.4. Unsupervised Editing

Next, we perform experiments using our unsupervised editing method. Here we set the classifier-free guidance strength to 3 for both SDEdit and our method. The strength of the modification is controlled by the parameter γ. As can be seen in Figs. 1(a),(b), 4, and 7, and can be listened to in Sec. 1.2 of our examples page, the modifications can range from effects like voice emphasis, to more stylistic changes *e.g.*, in a singer's vibrato. An interesting change is more apparent in music, where the semantic editing directions can take the form of an improvisation on the original piece, obtained by changing the melody, as shown in Fig. 4c.

The PCs of the posterior covariance convey the uncertainty of the denoising model at the current timestep. The synthesis process is inherently more uncertain at earlier timesteps in the sampling process (*i.e.*, at larger t). Therefore, the extracted directions $\{\mathbf{v}_{i|t}\}$ generally exhibit more global changes spread over larger segments of the samples for earlier timesteps, and more local changes for later timesteps. Empirically, above a certain timestep the extracted directions are not interesting. We therefore restrict ourselves here to $t \leq 135$ (see App. D for further discussion).

Qualitative comparisons can be listened to in Sec. 2.2 of our examples page. Quantifying unsupervised edits in music can

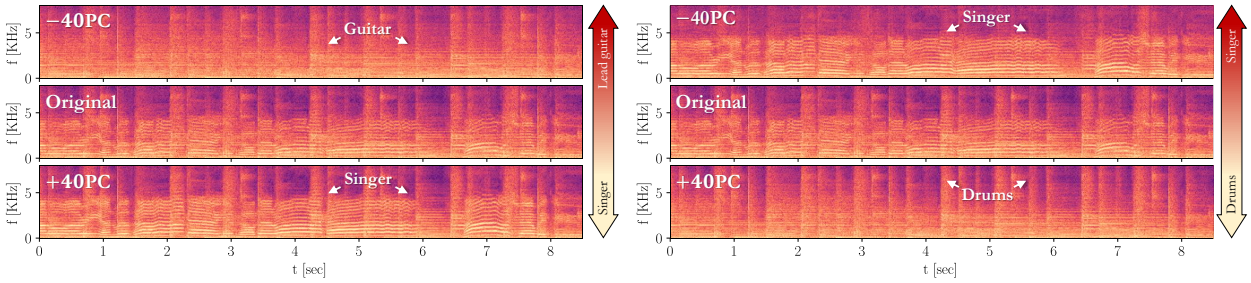

Figure 7. **The role of different PCs.** Our unsupervised editing method allows extracting different semantic editing directions for the same signal. These enable editing different semantic concepts that can complement each other. For example, the first PC shown here controls how much the singer is heard, at the expense of the lead guitar, while the second PC controls the whether the drums are dominant on the expense of the singer. Here $t' = t$, $T_{\text{start}} = 115$, and $T_{\text{end}} = 80$. This example can be listened to in Sec. 1.2.2 of our examples page.

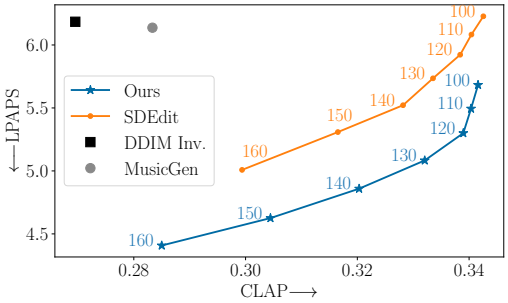

Figure 8. **Adherence to target prompt vs. fidelity to the original signal.** The plot compares MusicGen (Copet et al., 2023), SDEdit (Meng et al., 2021), DDIM Inversion and our method over the MusicDelta subset in MedleyDB (Bittner et al., 2014), using our prompts dataset. Our method and SDEdit are shown with T_{start} values ranging between 100 and 160. Our results achieve lower (better) LPAPS for any level of CLAP (higher is better), indicating a good balance between text adherence and signal fidelity.

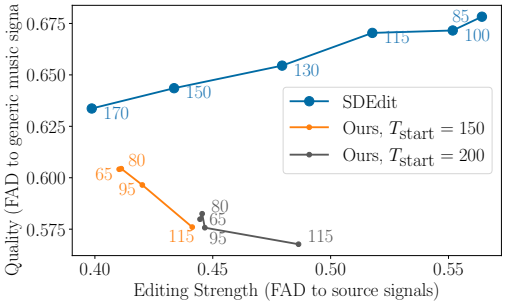

Figure 9. **Unsupervised editing strength vs. quality.** We compare SDEdit (Meng et al., 2021) to our method over the MusicDelta subset of MedleyDB (Bittner et al., 2014), using our prompts dataset. SDEdit is shown with T_{start} values ranging between 85 and 170, and our method is shown for different t' values (indicated on the plot) and T_{start} values (indicated in the legend). We use $T_{\text{end}} = 1$. For any level of perceptual deviation from the original signal, our method retains a higher quality (w.r.t. FMA-pop (Gui et al., 2024; Defferrard et al., 2017)).

be challenging as the editable aspects of music vary widely, from rhythm, melody, instrumentation, mood and genre. Therefore, for this task, LPAPS is less fitting for measuring the "strength" of an edit. Specifically, a semantically small change like a slight shift in rhythm that occurs across the entire signal can throw off LPAPS completely, even though it is barely perceived by humans. Similarly, a short melodic change will rank low on LPAPS distance, but can shift the perceived mood of the piece. Therefore, instead of LPAPS, here we measure the FAD to two different datasets. The first is the original Music Delta subset. This measures the strength of the edit, as it quantifies the deviation from the original distribution. The second is the FMA-pop dataset, a subset of FMA (Defferrard et al., 2017) proposed by Gui et al. (2024). This subset contains the 30 most popular songs for each of the 163 genres in the FMA dataset, and as such contains a large variety of genres and styles. This FAD gives an idea about the musical quality of the edited output on its own. We plot the two metrics in Fig. 9, using different T_{start} configurations for SDEdit and different t and t' values for our approach. Our method achieves a higher quality (lower FAD to general music) for any desired edit strength. See App. E for validation of the semantics of our directions, and App. F for their applicability in other domains, *e.g.*, images.

5. Conclusion

We presented two methods for zero-shot editing of audio signals using pre-trained diffusion models. To the best of our knowledge, this is the first attempt to fully explore zero-shot editing in the audio domain. In addition to a text-based method, which we adopted from the image domain, we proposed a novel unsupervised method for discovering editing directions. We demonstrated both qualitatively and quantitatively that our methods outperform other methods for text-based editing, and illustrated that our unsupervised method is able to create semantically meaningful modifications and improvisations to a source signal.

Impact Statement

The purpose of this paper is to advance the field of Machine Learning and in particular zero-shot editing of audio signals. We feel that there are many potential societal consequences of our work, but the predominant one relates to the ability of using our method for copyright infringement. In this work we intentionally chose to only work on audio licensed under Creative Commons Attribution, and as this is an academic work it is in fair use. However, as we publish our code users might use it to modify existing copyrighted musical pieces without sufficient permission of the copyright holder, and this might not fall under fair use under different circumstances. However, this is the case every editing work, presented in the image and video domains.

References

Agostinelli, A., Denk, T. I., Borsos, Z., Engel, J., Verzetti, M., Caillon, A., Huang, Q., Jansen, A., Roberts, A., Tagliasacchi, M., et al. MusicLM: Generating music from text. *arXiv preprint arXiv:2301.11325*, 2023. 1, 2, 6

Bittner, R., Salamon, J., Tierney, M., Mauch, M., Cannam, C., and Bello, J. MedleyDB: A multitrack dataset for annotation-intensive mir research. In *15th International Society for Music Information Retrieval Conference, ISMIR 2014*, 2014. 5, 8

Brooks, T., Holynski, A., and Efros, A. A. InstructPix2Pix: Learning to follow image editing instructions. In *Proceedings of the IEEE/CVF Conference on Computer Vision and Pattern Recognition (CVPR)*, pp. 18392–18402, June 2023. 1, 2

Cao, M., Wang, X., Qi, Z., Shan, Y., Qie, X., and Zheng, Y. MasaCtrl: Tuning-free mutual self-attention control for consistent image synthesis and editing. *arXiv preprint arXiv:2304.08465*, 2023. 3

Chen, H., Xie, W., Vedaldi, A., and Zisserman, A. VGGSound: A large-scale audio-visual dataset. In *ICASSP 2020-2020 IEEE International Conference on Acoustics, Speech and Signal Processing (ICASSP)*, pp. 721–725. IEEE, 2020. 6

Chen, K., Du, X., Zhu, B., Ma, Z., Berg-Kirkpatrick, T., and Dubnov, S. HTS-AT: A hierarchical token-semantic audio transformer for sound classification and detection. In *IEEE International Conference on Acoustics, Speech and Signal Processing, ICASSP*, 2022. 6, 12

Copet, J., Kreuk, F., Gat, I., Remez, T., Kant, D., Synnaeve, G., Adi, Y., and Défossez, A. Simple and controllable music generation. In *Thirty-seventh Conference on Neural Information Processing Systems*, 2023. 1, 2, 5, 7, 8, 12

Defferrard, M., Benzi, K., Vandergheynst, P., and Bresson, X. FMA: A dataset for music analysis. In *18th International Society for Music Information Retrieval Conference (ISMIR)*, 2017. 8

Dhariwal, P. and Nichol, A. Diffusion models beat gans on image synthesis. *Advances in neural information processing systems*, 34:8780–8794, 2021. 2, 3, 5

Gal, R., Alaluf, Y., Atzmon, Y., Patashnik, O., Bermano, A. H., Chechik, G., and Cohen-or, D. An image is worth one word: Personalizing text-to-image generation using textual inversion. In *The Eleventh International Conference on Learning Representations*, 2022. 1, 2

Ghosal, D., Majumder, N., Mehrish, A., and Poria, S. Text-to-audio generation using instruction guided latent diffusion model. In *Proceedings of the 31st ACM International Conference on Multimedia*, pp. 3590–3598, 2023. 1

Gui, A., Gamper, H., Braun, S., and Emmanouilidou, D. Adapting Frechet audio distance for generative music evaluation. In *Proc. IEEE ICASSP 2024*, 2024. 6, 8, 12

Haas, R., Huberman-Spiegelglas, I., Mulayoff, R., and Michaeli, T. Discovering interpretable directions in the semantic latent space of diffusion models. *arXiv preprint arXiv:2303.11073*, 2023. 3, 14

Han, B., Dai, J., Song, X., Hao, W., He, X., Guo, D., Chen, J., Wang, Y., and Qian, Y. InstructME: An instruction guided music edit and remix framework with latent diffusion models. *arXiv preprint arXiv:2308.14360*, 2023. 1, 2, 5

Hershey, S., Chaudhuri, S., Ellis, D. P., Gemmeke, J. F., Jansen, A., Moore, R. C., Plakal, M., Platt, D., Saurous, R. A., Seybold, B., et al. CNN architectures for large-scale audio classification. In *2017 ieee international conference on acoustics, speech and signal processing (icassp)*, pp. 131–135. IEEE, 2017. 6

Hertz, A., Mokady, R., Tenenbaum, J., Aberman, K., Pritch, Y., and Cohen-or, D. Prompt-to-prompt image editing with cross-attention control. In *The Eleventh International Conference on Learning Representations*, 2022. 3

Heusel, M., Ramsauer, H., Unterthiner, T., Nessler, B., and Hochreiter, S. GANs trained by a two time-scale update rule converge to a local nash equilibrium. *Advances in neural information processing systems*, 30, 2017. 6

Ho, J. and Salimans, T. Classifier-free diffusion guidance. In *NeurIPS 2021 Workshop on Deep Generative Models and Downstream Applications*, 2021. 4

Ho, J., Jain, A., and Abbeel, P. Denoising diffusion probabilistic models. *Advances in neural information processing systems*, 33:6840–6851, 2020. 1, 3

Huberman-Spiegelglas, I., Kulikov, V., and Michaeli, T. An edit friendly DDPM noise space: Inversion and manipulations. *arXiv preprint arXiv:2304.06140*, 2023. 1, 3, 4

Iashin, V. and Rahtu, E. Taming visually guided sound generation. In *British Machine Vision Conference (BMVC)*, 2021. 6

Jeong, J., Kwon, M., and Uh, Y. Training-free content injection using h-space in diffusion models. In *Proceedings of the IEEE/CVF Winter Conference on Applications of Computer Vision (WACV)*, pp. 5151–5161, January 2024. 3

Kawar, B., Zada, S., Lang, O., Tov, O., Chang, H., Dekel, T., Mosseri, I., and Irani, M. Imagic: Text-based real image editing with diffusion models. In *Proceedings of the IEEE/CVF Conference on Computer Vision and Pattern Recognition*, pp. 6007–6017, 2023. 1, 2

Kilgour, K., Zuluaga, M., Roblek, D., and Sharifi, M. Fr\'echet audio distance: A metric for evaluating music enhancement algorithms. *arXiv preprint arXiv:1812.08466*, 2018. 6

Kim, G., Kwon, T., and Ye, J. C. DiffusionCLIP: Text-guided diffusion models for robust image manipulation. In *Proceedings of the IEEE/CVF Conference on Computer Vision and Pattern Recognition*, pp. 2426–2435, 2022. 1

Kong, J., Kim, J., and Bae, J. HiFi-GAN: Generative adversarial networks for efficient and high fidelity speech synthesis. *Advances in Neural Information Processing Systems*, 33:17022–17033, 2020. 4

Kwon, M., Jeong, J., and Uh, Y. Diffusion models already have a semantic latent space. In *The Eleventh International Conference on Learning Representations*, 2022. 3

Liu, H., Chen, Z., Yuan, Y., Mei, X., Liu, X., Mandic, D., Wang, W., and Plumbley, M. D. AudioLDM: Text-to-audio generation with latent diffusion models. *Proceedings of the International Conference on Machine Learning*, 2023a. 1, 2, 4

Liu, H., Tian, Q., Yuan, Y., Liu, X., Mei, X., Kong, Q., Wang, Y., Wang, W., Wang, Y., and Plumbley, M. D. AudioLDM 2: Learning holistic audio generation with self-supervised pretraining. *arXiv preprint arXiv:2308.05734*, 2023b. 4, 5

Liu, Z., Lin, Y., Cao, Y., Hu, H., Wei, Y., Zhang, Z., Lin, S., and Guo, B. Swin transformer: Hierarchical vision transformer using shifted windows. In *Proceedings of the IEEE/CVF international conference on computer vision*, pp. 10012–10022, 2021. 7

Manor, H. and Michaeli, T. On the posterior distribution in denoising: Application to uncertainty quantification. In *The Twelfth International Conference on Learning Representations*, 2024. 1, 3, 4, 12, 13

Meng, C., He, Y., Song, Y., Song, J., Wu, J., Zhu, J.-Y., and Ermon, S. SDEdit: Guided image synthesis and editing with stochastic differential equations. In *International Conference on Learning Representations*, 2021. 1, 2, 5, 7, 8, 17, 20, 21

Nehme, E., Yair, O., and Michaeli, T. Uncertainty quantification via neural posterior principal components. In *Thirty-seventh Conference on Neural Information Processing Systems*, 2023. 4

Paissan, F., Wang, Z., Ravanelli, M., Smaragdis, P., and Subakan, C. Audio editing with non-rigid text prompts. *arXiv preprint arXiv:2310.12858*, 2023. 1, 2, 6

Park, Y.-H., Kwon, M., Jo, J., and Uh, Y. Unsupervised discovery of semantic latent directions in diffusion models. *arXiv preprint arXiv:2302.12469*, 2023. 3

Plitsis, M., Kouzelis, T., Paraskevopoulos, G., Katsouros, V., and Panagakis, Y. Investigating personalization methods in text to music generation. *arXiv preprint arXiv:2309.11140*, 2023. 1, 2, 5

Ramesh, A., Pavlov, M., Goh, G., Gray, S., Voss, C., Radford, A., Chen, M., and Sutskever, I. Zero-shot text-to-image generation. In *International Conference on Machine Learning*, pp. 8821–8831. PMLR, 2021. 1

Rombach, R., Blattmann, A., Lorenz, D., Esser, P., and Ommer, B. High-resolution image synthesis with latent diffusion models. In *Proceedings of the IEEE/CVF conference on computer vision and pattern recognition*, pp. 10684–10695, 2022. 1, 4, 17, 20, 21

Ruiz, N., Li, Y., Jampani, V., Pritch, Y., Rubinstein, M., and Aberman, K. DreamBooth: Fine tuning text-to-image diffusion models for subject-driven generation. In *Proceedings of the IEEE/CVF Conference on Computer Vision and Pattern Recognition*, pp. 22500–22510, 2023. 1, 2

Saad, Y. *Numerical methods for large eigenvalue problems: revised edition*. SIAM, 2011. 4, 13

Shen, Y. and Zhou, B. Closed-form factorization of latent semantics in GANs. In *Proceedings of the IEEE/CVF Conference on Computer Vision and Pattern Recognition (CVPR)*, pp. 1532–1540, June 2021. 3

Shen, Y., Gu, J., Tang, X., and Zhou, B. Interpreting the latent space of gans for semantic face editing. In *Proceedings of the IEEE/CVF conference on computer vision and pattern recognition*, pp. 9243–9252, 2020. 3

Sohl-Dickstein, J., Weiss, E., Maheswaranathan, N., and Ganguli, S. Deep unsupervised learning using nonequilibrium thermodynamics. In *International conference on machine learning*, pp. 2256–2265. PMLR, 2015. 1

Song, J., Meng, C., and Ermon, S. Denoising diffusion implicit models. *arXiv preprint arXiv:2010.02502*, 2020. 1

Song, J., Meng, C., and Ermon, S. Denoising diffusion implicit models. In *International Conference on Learning Representations*, 2021. 2, 3, 5

Spingarn, N., Banner, R., and Michaeli, T. GAN "steerability" without optimization. In *International Conference on Learning Representations*, 2020. 3

Tumanyan, N., Geyer, M., Bagon, S., and Dekel, T. Plug-and-play diffusion features for text-driven image-to-image translation. In *Proceedings of the IEEE/CVF Conference on Computer Vision and Pattern Recognition*, pp. 1921–1930, 2023. 1, 3, 17, 20, 21

Wang, Y., Ju, Z., Tan, X., He, L., Wu, Z., Bian, J., and sheng zhao. AUDIT: Audio editing by following instructions with latent diffusion models. In *Thirty-seventh Conference on Neural Information Processing Systems*, 2023. 1, 2, 5

Wu, C. H. and De la Torre, F. A latent space of stochastic diffusion models for zero-shot image editing and guidance. In *Proceedings of the IEEE/CVF International Conference on Computer Vision*, pp. 7378–7387, 2023. 1, 3

Wu, Y., Chen, K., Zhang, T., Hui, Y., Berg-Kirkpatrick, T., and Dubnov, S. Large-scale contrastive language-audio pretraining with feature fusion and keyword-to-caption augmentation. In *IEEE International Conference on Acoustics, Speech and Signal Processing, ICASSP*, 2023. 6, 12

Wu, Z., Lischinski, D., and Shechtman, E. StyleSpace analysis: Disentangled controls for stylegan image generation. In *Proceedings of the IEEE/CVF Conference on Computer Vision and Pattern Recognition*, pp. 12863–12872, 2021. 3

Zhang, C., Ren, Y., Zhang, K., and Yan, S. SDMuse: Stochastic differential music editing and generation via hybrid representation. *IEEE Transactions on Multimedia*, 2023a. 3

Zhang, R., Isola, P., Efros, A. A., Shechtman, E., and Wang, O. The unreasonable effectiveness of deep features as a perceptual metric. In *Proceedings of the IEEE conference on computer vision and pattern recognition*, pp. 586–595, 2018. 6

Zhang, Z., Han, L., Ghosh, A., Metaxas, D. N., and Ren, J. SINE: Single image editing with text-to-image diffusion models. In *Proceedings of the IEEE/CVF Conference on Computer Vision and Pattern Recognition*, pp. 6027–6037, 2023b. 1

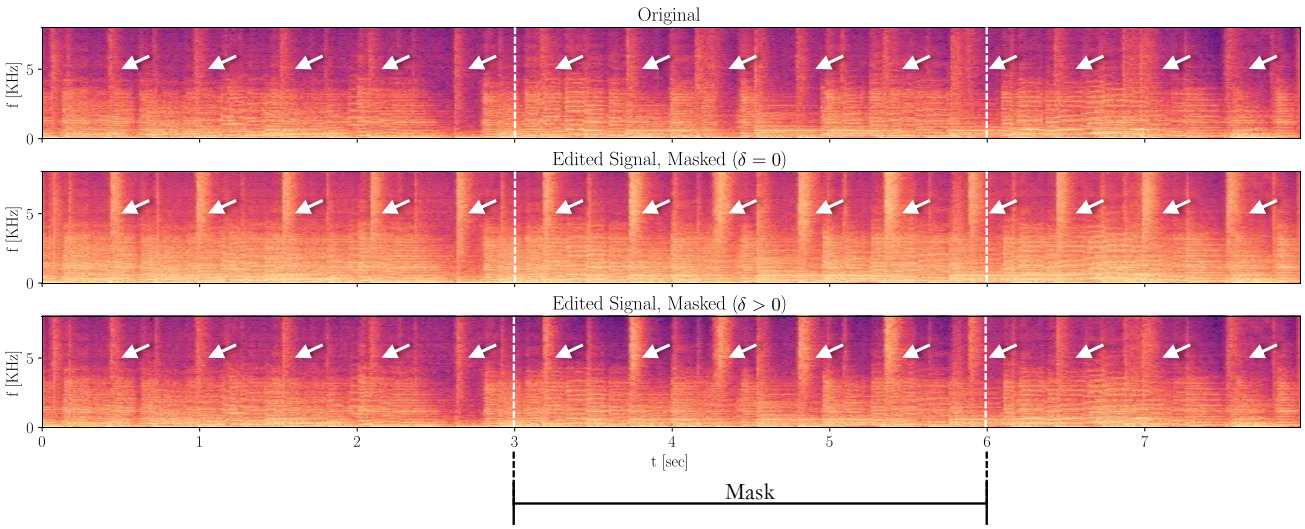

Figure 10. **Example of data leakage in diffusion models editing.** The extracted PC affects the snare of the drums beats, marked with arrows. By shifting the parts of the signal outside the mask closer to the original signal at each timestep, the snare only changes in the masked region. By not shifting the signal, the snare changes along the entire signal.

A. Experimental Details

For the CLAP model used in the CLAP, LPAPS, and FAD metrics calculation, as described in Sec. 4.2, we follow Gui et al. (2024) and MusicGen (Copet et al., 2023), and use the "music_audioset_epoch_15_esc_90.14.pt" checkpoint of LAION-AI (Chen et al., 2022; Wu et al., 2023).

In all of our unsupervised editing experiments, we run 50 subspace iterations for extracting PCs, and set $C = 10^{-3}$ as the small approximation constant as described by Manor & Michaeli (2024). We use MusicGen with their default parameters provided in their official implementation demo. Additionally, we opt to not use negative prompts in all experiments.

B. Editing Over a User-Chosen Segment

Editing can be confined to a user-chosen segment, rather than the whole signal, by using a mask during the generative process. When doing so, at each timestep t, after computing $\mathbf{x}_{t-1}$ using (1) or (5), for text-based editing and unsupervised editing respectively, we enforce the parts of the signal outside the mask to shift back closer to the original signal at that timestep. We do this by setting

$$\mathbf{x}_{t-1} \leftarrow M \odot \mathbf{x}_{t-1} + (1 - M) \odot (\delta \mathbf{x}_{t-1}^{\text{orig}} + (1 - \delta)\mathbf{x}_{t-1}), \tag{6}$$

where M is the mask, and δ is some small constant which we fix to 0.025 in all experiments.

This shift is necessary due to "data leakage" caused by the architecture of the diffusion model. The term data leakage refers to the phenomenon where a localized edit, *e.g.*, a PC calculated for a specific segment of the signal using a mask, unintentionally affects the rest of the signal. This is commonly caused by the use of a UNet and attention modules as backbones for the diffusion model. The effect of the data leakage can be viewed in Fig. 10. The extracted PC at this timestep, $t = 80$, affects the snare of the drums beats. Without shifting the parts outside the mask back to the original signal, the snare changes across the entire signal. By setting $\delta > 0$ the change is localized to the masked region.

We notice empirically that the strength of the data leakage depends on the type of edit, however, generally it is not known a priori. Additionally, we would like to note that setting $\delta > 0$ is application specific and its effect is subjective. On the one hand, using a mask implies that changes outside the mask region are unwanted. However, allowing the edit to have a more global influence across the entire signal, could result in a more consistent result (*e.g.*, it might make more sense that the drum beats' snare changes across an entire musical piece).

C. Unsupervised Editing Implementation Details

Consider the multivariate denoising problem observation $\mathbf{y} = \mathbf{x} + \mathbf{n}$, where $\mathbf{x}$ is a random vector and the noise $\mathbf{n} \sim \mathcal{N}(0, \sigma^2)$ is statistically independent of $\mathbf{x}$. Then, Manor & Michaeli (2024) show that the posterior covariance relates to the Jacobian of an MSE-optimal denoiser,

$$\mathrm{Cov}[\mathbf{x}|\mathbf{y} = \boldsymbol{y}] = \sigma^2 \frac{\partial \mathbb{E}[\mathbf{x}|\mathbf{y} = \boldsymbol{y}]}{\partial \boldsymbol{y}}, \tag{7}$$

where $\boldsymbol{y}$ is the noisy sample. The work further showed that extracting the top eigenvectors and eigenvalues of the posterior covariance can be done using the subspace iteration method (Saad, 2011), where each iteration can be approximated using a single forward pass through the denoiser network.

In DDMs, Eq. (2) can be rearranged to fit the aforementioned observation model:

$$\frac{\mathbf{x}_t}{\sqrt{\bar{\alpha}_t}} = \mathbf{x}_0 + \frac{\sqrt{1-\bar{\alpha}_t}}{\sqrt{\bar{\alpha}_t}} \boldsymbol{\epsilon}_t, \quad t = 1, \ldots, T. \tag{8}$$

Therefore, $\mathbf{x} = \mathbf{x}_0$, $\mathbf{y} = \mathbf{x}_t/\sqrt{\bar{\alpha}_t}$, and $\mathbf{n} \sim \mathcal{N}(0, (1-\bar{\alpha}_t)/\bar{\alpha}_t \boldsymbol{I})$. Under this point of view, each timestep t in the diffusion process is a Gaussian denoising problem, and we get

$$\begin{aligned} \mathrm{Cov}\left[\mathbf{x}_0 \middle| \frac{\mathbf{x}_t}{\sqrt{\bar{\alpha}_t}}\right] &= \frac{1-\bar{\alpha}_t}{\bar{\alpha}_t} \cdot \frac{\partial \mathbb{E}\left[\mathbf{x}_0 \middle| \frac{\mathbf{x}_t}{\sqrt{\bar{\alpha}_t}}\right]}{\partial \frac{\mathbf{x}_t}{\sqrt{\bar{\alpha}_t}}} \\ \mathrm{Cov}\left[\mathbf{x}_0 | \mathbf{x}_t\right] &= \frac{1-\bar{\alpha}_t}{\bar{\alpha}_t} \cdot \frac{\partial \mathbb{E}\left[\mathbf{x}_0 | \mathbf{x}_t\right]}{\partial \mathbf{x}_t}. \end{aligned} \tag{9}$$

This allows for using the algorithm proposed by Manor & Michaeli (2024) at every desired timestep t' of the diffusion model, to extract semantic directions $\{\mathbf{v}_{i|t'}\}$ and their corresponding factors $\{\lambda_{i|t'}\}$.

These directions are PCs of the posterior covariance, and as such they need to be added to the primal space, and in particular to $\hat{\mathbf{x}}_{0|t'}$. As described in Sec. 3.1, the reverse process of a diffusion model is written in Eq. (1) as $\mathbf{x}_{t-1} = \boldsymbol{\mu}_t(\mathbf{x}_t) + \sigma_t \mathbf{z}_t$, where $\{\mathbf{z}_t\}_{t=1}^T \sim \mathcal{N}(0, \boldsymbol{I})$, $\mathbf{z}_0 = 0$, $\{\sigma_t\}$ is an increasing sequence of noise levels, and $\boldsymbol{\mu}_t(\mathbf{x}_t)$ is a function of a neural network trained to predict $\boldsymbol{\epsilon}_t$ from $\mathbf{x}_t$.

This function can be expressed as the sum of two elements:

$$\boldsymbol{\mu}_t = \sqrt{\bar{\alpha}_{t-1}} \boldsymbol{P}\big(\mathbf{f}_t(\mathbf{x}_t)\big) + \boldsymbol{D}\big(\mathbf{f}_t(\mathbf{x}_t)\big). \tag{10}$$

Here, $\mathbf{f}_t(\mathbf{x}_t)$ is the aforementioned neural network trained to predict $\boldsymbol{\epsilon}_t$ from $\mathbf{x}_t$. $\boldsymbol{P}\big(\mathbf{f}_t(\mathbf{x}_t)\big)$ is given by

$$\boldsymbol{P}\big(\mathbf{f}_t(\mathbf{x}_t)\big) = \big(\mathbf{x}_t - \sqrt{1-\bar{\alpha}_t}\mathbf{f}_t(\mathbf{x}_t)\big)/\sqrt{\bar{\alpha}_t}, \tag{11}$$

and is the predicted $\mathbf{x}_0$ at timestep t, noted as $\hat{\mathbf{x}}_{0|t}$. $\boldsymbol{D}\big(\mathbf{f}_t(\mathbf{x}_t)\big)$ is the direction pointing to $\mathbf{x}_t$, given by

$$\boldsymbol{D}\big(\mathbf{f}_t(\mathbf{x}_t)\big) = \sqrt{1-\bar{\alpha}_{t-1}-\sigma_t^2}\mathbf{f}_t(\mathbf{x}_t). \tag{12}$$

Note that $\boldsymbol{P}\big(\mathbf{f}_t(\mathbf{x}_t)\big)$ gives a simple connection between $\hat{\mathbf{x}}_{0|t}$ and $\mathbf{f}_t(\mathbf{x}_t)$, the neural network, and therefore changing one is equivalent to changing another. Specifically, suppose we apply an edit to $\boldsymbol{\mu}_t$ by adding $\gamma\sqrt{\lambda_{i|t}}\mathbf{v}_{i|t'}$ to $\hat{\mathbf{x}}_{0|t}$ in Eq. (10). We denote this edited $\boldsymbol{\mu}_t$ as $\boldsymbol{\mu}_t^{\text{edit}}$:

$$\boldsymbol{\mu}_t^{\text{edit}}(\mathbf{x}_t) = \sqrt{\bar{\alpha}_{t-1}}\Big(\boldsymbol{P}\big(\mathbf{f}_t(\mathbf{x}_t)\big) + \gamma\sqrt{\lambda_{i|t}}\mathbf{v}_{i|t'}\Big) + \boldsymbol{D}\big(\mathbf{f}_t(\mathbf{x}_t)\big). \tag{13}$$

By substituting Eq. (11) into Eq. (13) we get

$$\begin{aligned}
\boldsymbol{\mu}_t^{\text{edit}}(\mathbf{x}_t) &= \sqrt{\bar{\alpha}_{t-1}}\Big(\frac{\mathbf{x}_t - \sqrt{1-\bar{\alpha}_t}\mathbf{f}_t(\mathbf{x}_t)}{\sqrt{\bar{\alpha}_t}} + \gamma\sqrt{\lambda_{i|t}}\mathbf{v}_{i|t'}\Big) + \boldsymbol{D}\big(\mathbf{f}_t(\mathbf{x}_t)\big) \\
&= \sqrt{\bar{\alpha}_{t-1}} \cdot \frac{\mathbf{x}_t - \sqrt{1-\bar{\alpha}_t}\mathbf{f}_t(\mathbf{x}_t) + \gamma\sqrt{\bar{\alpha}_t}\sqrt{\lambda_{i|t}}\mathbf{v}_{i|t'}}{\sqrt{\bar{\alpha}_t}} + \boldsymbol{D}\big(\mathbf{f}_t(\mathbf{x}_t)\big) \\
&= \sqrt{\bar{\alpha}_{t-1}} \cdot \frac{\mathbf{x}_t - \sqrt{1-\bar{\alpha}_t}\big(\mathbf{f}_t(\mathbf{x}_t) - \gamma\frac{\sqrt{\bar{\alpha}_t}}{\sqrt{1-\bar{\alpha}_t}}\sqrt{\lambda_{i|t}}\mathbf{v}_{i|t'}\big)}{\sqrt{\bar{\alpha}_t}} + \boldsymbol{D}\big(\mathbf{f}_t(\mathbf{x}_t)\big) \\
&= \sqrt{\bar{\alpha}_{t-1}}\boldsymbol{P}\Big(\mathbf{f}_t(\mathbf{x}_t) - \gamma\frac{\sqrt{\bar{\alpha}_t}}{\sqrt{1-\bar{\alpha}_t}}\sqrt{\lambda_{i|t}}\mathbf{v}_{i|t'}\Big) + \boldsymbol{D}\big(\mathbf{f}_t(\mathbf{x}_t)\big). \qquad (14)
\end{aligned}$$

This is an asymmetric reverse process formulation (Asyrp), since the two functions $\boldsymbol{P}$ and $\boldsymbol{D}$ that compose $\boldsymbol{\mu}_t^{\text{edit}}$ are operating on different variables. A symmetric reverse process is then given by also changing $\boldsymbol{D}\big(\mathbf{f}_t(\mathbf{x}_t)\big)$ accordingly,

$$\boldsymbol{\mu}_t^{\text{edit}}(\mathbf{x}_t) = \sqrt{\bar{\alpha}_{t-1}}\boldsymbol{P}\Big(\mathbf{f}_t(\mathbf{x}_t) - \gamma\frac{\sqrt{\bar{\alpha}_t}}{\sqrt{1-\bar{\alpha}_t}}\sqrt{\lambda_{i|t}}\mathbf{v}_{i|t'}\Big) + \boldsymbol{D}\Big(\mathbf{f}_t(\mathbf{x}_t) - \gamma\frac{\sqrt{\bar{\alpha}_t}}{\sqrt{1-\bar{\alpha}_t}}\sqrt{\lambda_{i|t}}\mathbf{v}_{i|t'}\Big). \qquad (15)$$

This means effectively subtracting $\gamma\frac{\sqrt{\bar{\alpha}_t}}{\sqrt{1-\bar{\alpha}_t}}\sqrt{\lambda_{i|t}}\mathbf{v}_{i|t'}$ from the noise prediction network output. Similar to Haas et al. (2023), we empirically find that the difference between the two formulations only changes the amplification of the editing effect, and therefore opt to use a symmetric reverse process for simplicity.

Finally, we can write $\boldsymbol{\mu}_t^{\text{edit}}$ explicitly by using both Eq. (11) and Eq. (12):

$$\begin{aligned}
\boldsymbol{\mu}_t^{\text{edit}}(\mathbf{x}_t) &= \sqrt{\bar{\alpha}_{t-1}}\Big(\frac{\mathbf{x}_t - \sqrt{1-\bar{\alpha}_t}\mathbf{f}_t(\mathbf{x}_t)}{\sqrt{\bar{\alpha}_t}} + \gamma\sqrt{\lambda_{i|t}}\mathbf{v}_{i|t'}\Big) + \sqrt{1-\bar{\alpha}_{t-1}-\sigma_t^2}\Big(\mathbf{f}_t(\mathbf{x}_t) - \gamma\frac{\sqrt{\bar{\alpha}_t}}{\sqrt{1-\bar{\alpha}_t}}\sqrt{\lambda_{i|t}}\mathbf{v}_{i|t'}\Big) \\
&= \sqrt{\bar{\alpha}_{t-1}}\Big(\frac{\mathbf{x}_t - \sqrt{1-\bar{\alpha}_t}\mathbf{f}_t(\mathbf{x}_t)}{\sqrt{\bar{\alpha}_t}}\Big) + \gamma\sqrt{\bar{\alpha}_{t-1}}\sqrt{\lambda_{i|t}}\mathbf{v}_{i|t'} \\
&\qquad + \sqrt{1-\bar{\alpha}_{t-1}-\sigma_t^2}\mathbf{f}_t(\mathbf{x}_t) - \gamma\sqrt{1-\bar{\alpha}_{t-1}-\sigma_t^2}\frac{\sqrt{\bar{\alpha}_t}}{\sqrt{1-\bar{\alpha}_t}}\sqrt{\lambda_{i|t}}\mathbf{v}_{i|t'} \\
&= \sqrt{\bar{\alpha}_{t-1}}\boldsymbol{P}\big(\mathbf{f}_t(\mathbf{x}_t)\big) + \boldsymbol{D}\big(\mathbf{f}_t(\mathbf{x}_t)\big) + \gamma\sqrt{\lambda_{i|t}}\mathbf{v}_{i|t'}\Big(\sqrt{\bar{\alpha}_{t-1}} - \sqrt{1-\bar{\alpha}_{t-1}-\sigma_t^2}\frac{\sqrt{\bar{\alpha}_t}}{\sqrt{1-\bar{\alpha}_t}}\Big) \\
&= \boldsymbol{\mu}_t(\mathbf{x}_t) + \gamma\sqrt{\lambda_{i|t}}\mathbf{v}_{i|t'} \cdot \Big(\sqrt{\bar{\alpha}_{t-1}} - \frac{\sqrt{\bar{\alpha}_t}}{\sqrt{1-\bar{\alpha}_t}}\sqrt{1-\bar{\alpha}_{t-1}-\sigma_t^2}\Big). \qquad (16)
\end{aligned}$$

Then, by setting

$$c_t = \sqrt{\bar{\alpha}_{t-1}} - \frac{\sqrt{\bar{\alpha}_t}}{\sqrt{1-\bar{\alpha}_t}}\sqrt{1-\bar{\alpha}_{t-1}-\sigma_t^2}, \qquad (17)$$

we get Eq. (5):

$$\mathbf{x}_{t-1} = \boldsymbol{\mu}_t(\mathbf{x}_t) + \gamma c_t \lambda_{i|t}^{1/2}\mathbf{v}_{i|t'} + \sigma_t\mathbf{z}_t, \quad t = T, \ldots, 1.$$

PCs computed using subspace iterations for each timestep separately are calculated independently of one another. As such, PCs for adjacent timesteps might be highly correlated. This is because in adjacent timesteps the noise level and uncertainty level are similar. Specifically, PCs from adjacent timesteps might be highly negatively correlated, as the positive directions are independently chosen at each timesteps. As explained in Sec. 3.3, one way of editing using Eq. (5) involves setting $t' = t$, so that each denoising step is perturbed with its own PCs. Therefore, it is possible that when perturbing the signal using PCs from neighboring timesteps they will cancel each other, thereby lessening the editing effect. To that end, at the end of the PCs computation for each timestep we compare the current PCs, $\mathbf{v}_{i|t}$, to those calculated during the previous timestep, $\mathbf{v}_{i|t+1}$. When the PCs correlation is lower than some threshold $\rho < 0$, we swap the direction of the current PCs, $\mathbf{v}_{i|t}$.

In addition to publishing the code repository, we provide in Alg. 1 the complete algorithm for the unsupervised PC computation described here and in Sec. 3.3 for reference.

Algorithm 1 Unsupervised PCs Computation

Inputs:
  Timesteps to extract PCs for $\{T_{\text{start}}, \dots, T_{\text{end}}\}$,
  Inverted noise vectors $\{\mathbf{x}_{T_{\text{start}}}, \mathbf{z}_{T_{\text{start}}}, \dots, \mathbf{z}_{T_{\text{end}}}\}$,
  Number of PCs N,
  DDPM Denoiser $\mathbf{f}_t(\cdot)$,
  coefficients $\{\bar{\alpha}_{T_{\text{start}}}, \dots, \bar{\alpha}_{T_{\text{end}}}\}$,
  noise-levels $\{\sigma_{T_{\text{start}}}, \dots, \sigma_{T_{\text{end}}}\}$,
  Threshold for correlation swap ρ,
  Approximation constant $C \ll 1$,
  Iterations amount K

Initialize $\mathbf{x}_t \leftarrow \mathbf{x}_{T_{\text{start}}}$
for $t \leftarrow T_{\text{start}}$ to T_{end} **do**
  $\mathbf{x}_{0|t} \leftarrow \left(\mathbf{x}_t - \sqrt{1-\bar{\alpha}_t}\mathbf{f}_t(\mathbf{x}_t)\right)/\sqrt{\bar{\alpha}_t}$ {Run a normal reverse pass.}
  $\boldsymbol{\mu}_t \leftarrow \sqrt{\bar{\alpha}_{t-1}}\mathbf{x}_{0|t} + \sqrt{1-\bar{\alpha}_{t-1}-\sigma_t^2}\mathbf{f}_t(\mathbf{x}_t)$
  $\mathbf{x}_{t-1} \leftarrow \boldsymbol{\mu}_t + \sigma_t \mathbf{z}_t$
  $\{\mathbf{v}_{i|t}^{(0)}\}_{i=1}^{N} \leftarrow \mathcal{N}(0, \boldsymbol{I})$ {Extract PCs using K subspace iterations over $\mathbf{x}_{0|t}$.}
  for $k \leftarrow 1$ to K **do**
    for $i \leftarrow 1$ to N **do**
      $\mathbf{x}_t^{\text{shifted}} \leftarrow \mathbf{x}_t + C\sqrt{\bar{\alpha}_t}\mathbf{v}_{i|t}^{(k-1)}$
      $\mathbf{x}_{0|t}^{\text{shifted}} \leftarrow \left(\mathbf{x}_t^{\text{shifted}} - \sqrt{1-\bar{\alpha}_t}\mathbf{f}_t(\mathbf{x}_t^{\text{shifted}})\right)/\sqrt{\bar{\alpha}_t}$
      $\mathbf{v}_{i|t}^{(k)} \leftarrow \frac{1}{C}\left(\mathbf{x}_{0|t}^{\text{shifted}} - \mathbf{x}_{0|t}\right)$
    end for
    $\mathbf{Q}, \mathbf{R} \leftarrow$ QR_Decomposition($[\mathbf{v}_{1|t}^{(k)} \cdots \mathbf{v}_{N|t}^{(k)}]$)
    $[\mathbf{v}_{1|t}^{(k)} \cdots \mathbf{v}_{N|t}^{(k)}] \leftarrow \mathbf{Q}$
  end for
  $\mathbf{v}_{i|t} \leftarrow \mathbf{v}_{i|t}^{(K)}$ {Save the computed PCs and EVs for timestep t.}
  $\lambda_{i|t} \leftarrow \frac{1/\bar{\alpha}_t - 1}{C}\left\|\mathbf{x}_{0|t}^{\text{shifted}} - \mathbf{x}_{0|t}\right\|$
  for $i \leftarrow 1$ to N **do**
    if $\mathbf{v}_{i|t} \cdot \mathbf{v}_{i|t+1} < \rho$ **then**
      $\mathbf{v}_{i|t} \leftarrow -\mathbf{v}_{i|t}$ {Swap the PCs direction if it is highly negatively correlated with the previous PC.}
    end if
  end for
  $\mathbf{x}_t \leftarrow \mathbf{x}_{t-1}$
end for

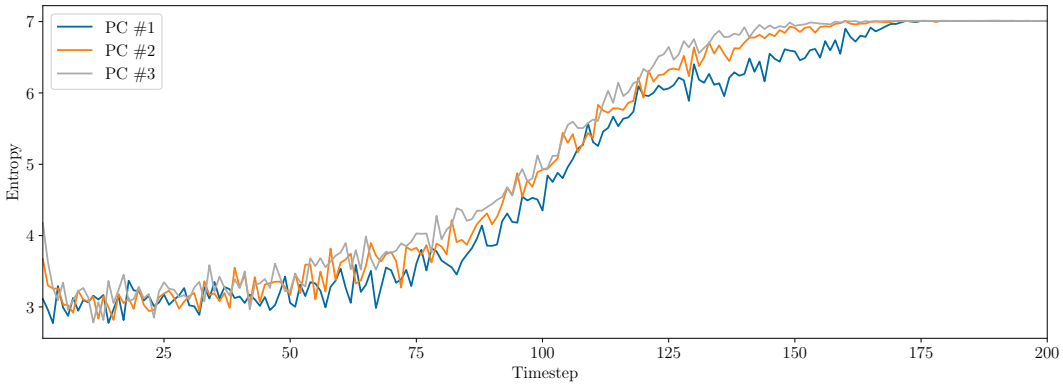

Figure 11. **Average entropy of the extracted PCs, across different timesteps.** Higher entropy is an indicator for global PCs, that change large segments of the signal. As the reverse process continues, the uncertainty in $\hat{\mathbf{x}}_{0|t}$ decreases, and the extracted PCs affect more localized areas, and measure lower in entropy.

D. The Effect of Using PCs From Different Timesteps $\{t'\}$

As mentioned in Sec. 4.4, modifications resulting from different choices of $\{t'\}$ vary in their extent of global impact. This can be measured quantitatively by calculating the entropy of the PC when summing over the different channels and height of the tensors. Fig. 11 displays the average entropy results for the first 3 PCs over the MusicDelta subset dataset used in the paper. Global changes that spread across large segments of the signal are characterized by a higher entropy, whereas lower entropy is an indicator for localized modifications. As can be seen, the entropy decays for smaller timesteps (later timesteps in the reverse diffusion process).

Empirically we see that the ability of the subspace iteration method to converge at large timesteps is hampered. This is also visible in Fig. 11, where the entropy is constant in the earliest timesteps. The uncertainty at the start of the diffusion process is very large, which coincides with the existence of multiple PCs with similar strength, *i.e.*, there are no dominant directions. The subspace iteration method performs worse in such cases and is slower, and as such the extracted directions at earlier timesteps are not very interesting. We also note that timesteps so early in the diffusion process are responsible for very global semantics, therefore editing them will result in a very large deviation from the original signal. Effectively, editing using those timesteps is equivalent to synthesizing a signal almost from scratch instead of editing it, which is not the desired task. As the reverse process continues the uncertainty decreases, the signal's general structure is set, and the PCs display more fine-grained directions of editing.

E. Comparison of Unsupervised Editing Directions With Random Directions

To ensure our computed PCs are significant and do indeed carry semantic meaning, we compare them to random directions in Fig. 12, Fig. 13 and Fig. 14. Specifically, we compare for multiple signals the 1^{st} PC computed using our method, or a combination of the first 3 PCs, using both editing ways: (i) Applying a specific timestep t' and adding it to a range of timesteps $[T_{\text{start}}, \ldots, T_{\text{end}}]$, and (ii) setting $t' = t$ when adding the PCs to a range of timesteps. When using a specific timestep, t', across a range of timesteps, $[T_{\text{start}}, \ldots, T_{\text{end}}]$, we sample a random direction from an isotropic Gaussian distribution. When settings $t' = t$, we randomly sample a direction for each timestep in the range $[T_{\text{start}}, \ldots, T_{\text{end}}]$, sampled i.i.d from an isotropic Gaussian distribution. In both cases, we normalize the randomly sampled directions to share the same norm as our directions, the unit-norm, and use the same computed eigenvalues $\lambda_{i|t}^{1/2}$ in Eq. (5).

Our computed PCs display semantically meaningful editing directions, while using random directions over the strength γ introduces almost imperceptible changes. Using a large γ factor introduces random changes that rapidly degrade the quality of the modification. All examples can be listened to in Sec. 3 of our examples page.

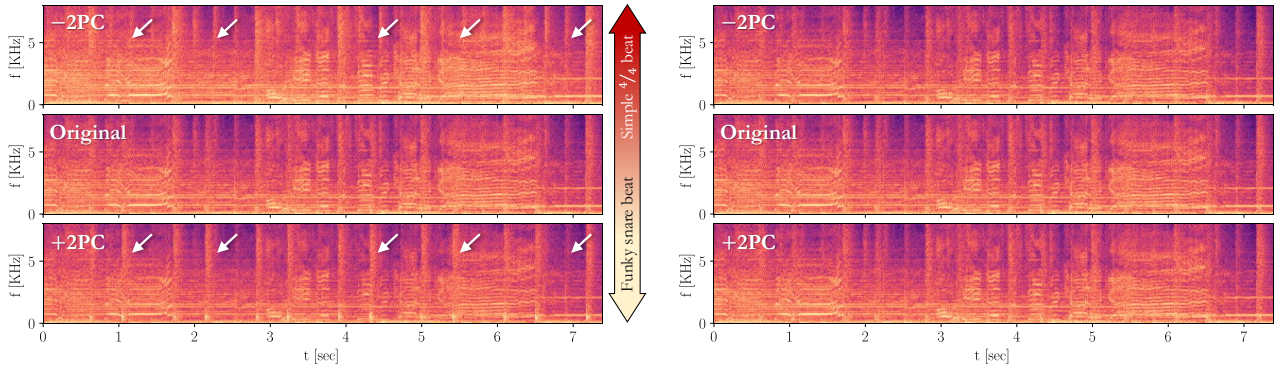

(a) The first PC computed using our method, $\gamma = 2$.

(b) Random direction, $\gamma = 2$.

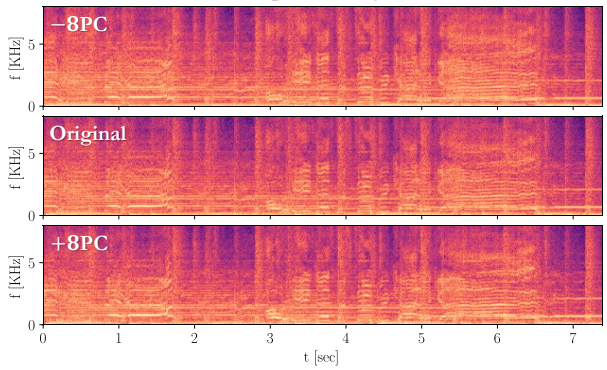

(c) Random direction, $\gamma = 8$.

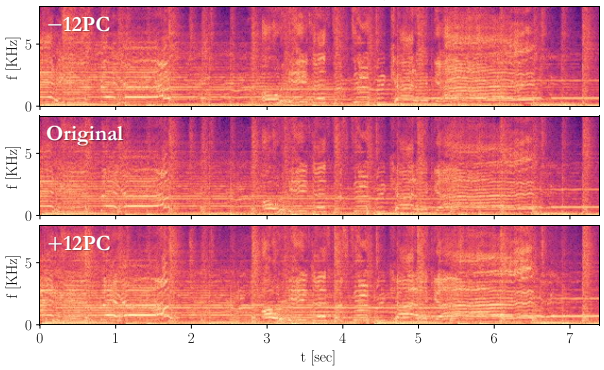

(d) Random direction, $\gamma = 12$.

Figure 12. **Our 1^{st} PC vs. a random direction.** While our method extract PCs with a clear semantic meaning (12a), *e.g.*, changing the drums beat style from a simple 4/4 beat to a syncopated (off-beat) and snare-heavy beat, the effect of using random directions (12b),(12c),(12d) varies from producing unnoticeable changes with small γ factor to degrading the signal when large γ values are used. This result can be listened to in Sec. 3 of our examples page. We fix here $t' = 80$ for our method, and apply our or the random directions for $T_{\text{start}} = 200$, $T_{\text{end}} = 1$. Both samples were generated using the music checkpoint of AudioLDM2, with a source prompt randomly chosen from our prompts dataset.

F. Unsupervised Editing in Images

We demonstrated our novel unsupervised editing approach on audio signals, since when applied on music it exposes a range of musically interesting modifications, some of which are virtually impossible to describe by text precisely. However, this approach is not limited to the audio domain. As a preliminary demonstration of its generalization ability, we leverage Stable Diffusion (Rombach et al., 2022) to demonstrate in Figs. 15, 16 and Fig. 17 semantic editing directions extracted for images from "modified ImageNet-R-TI2I" (Tumanyan et al., 2023), and contrast the results with both the well known SDEdit (Meng et al., 2021) and our previously proposed random baseline (See App. E). Our editing directions encode meaningful direction that change semantic elements while keepin the rest of the images, both its essence (*e.g.*, a sketch of a cat) and its structure intact.

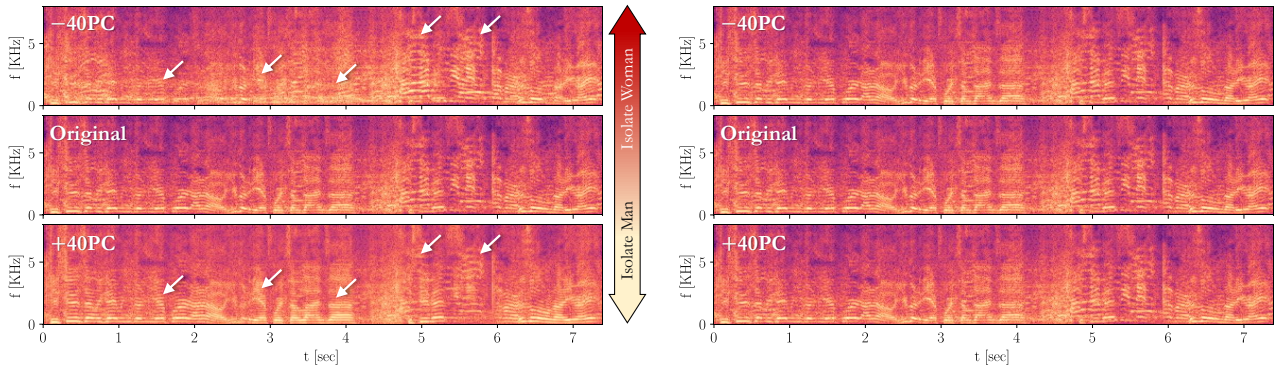

(a) The first PC computed using our method, , $\gamma = 40$.

(b) Random direction, $\gamma = 40$.

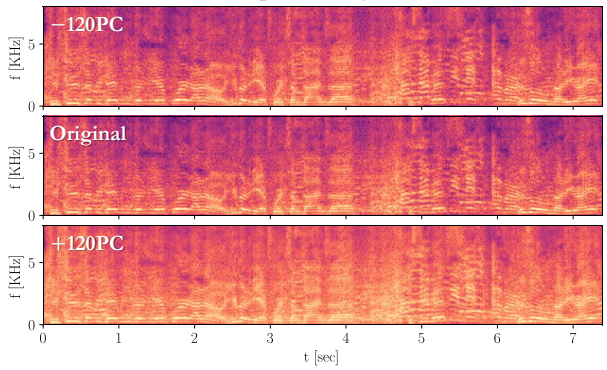

(c) Random direction, $\gamma = 120$.

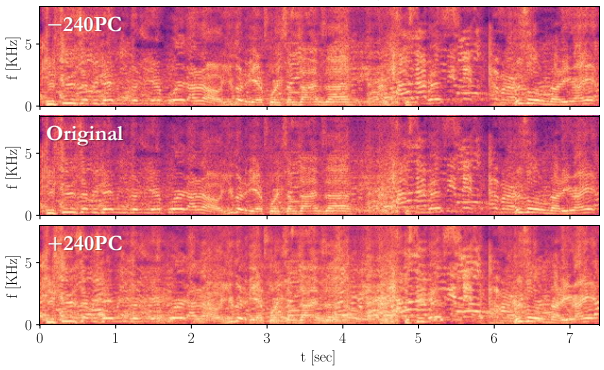

(d) Random direction, $\gamma = 240$.

Figure 13. **Our 1^{st} PC vs. a random direction.** While our method extract PCs with a clear semantic meaning (13a), *e.g.*, isolating a man or a woman speaking in a given signal, the effect of using random directions (13b),(13c),(13d) varies from producing unnoticeable changes with small γ factor to degrading the signal when large γ values are used. This result can be listened to in Sec. 3 of our examples page. We fix $t' = t$, and apply our or the random directions for $T_{\text{start}} = 115$, $T_{\text{end}} = 95$. Both samples were generated using the large checkpoint of AudioLDM2, without a source prompt.

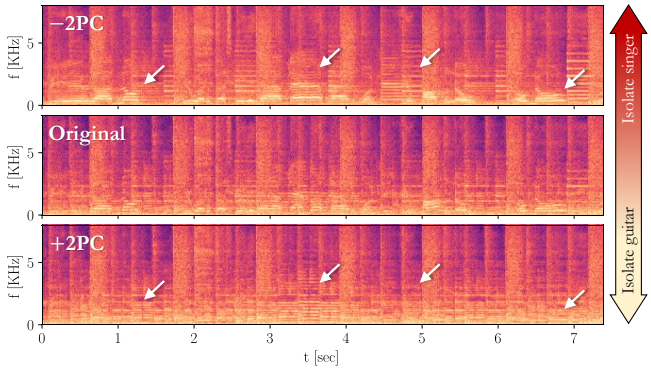

(a) The first 3 PCs combined computed using our method, $\gamma = 2$.

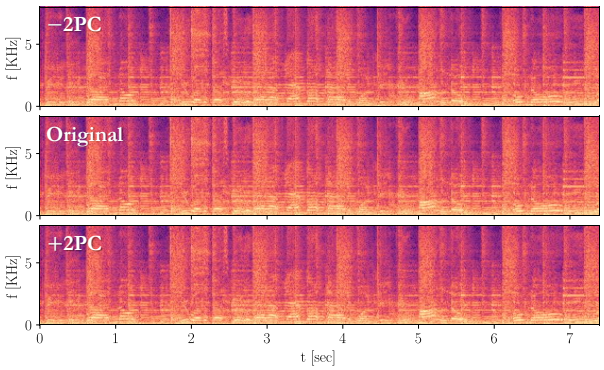

(b) Random directions, $\gamma = 2$.

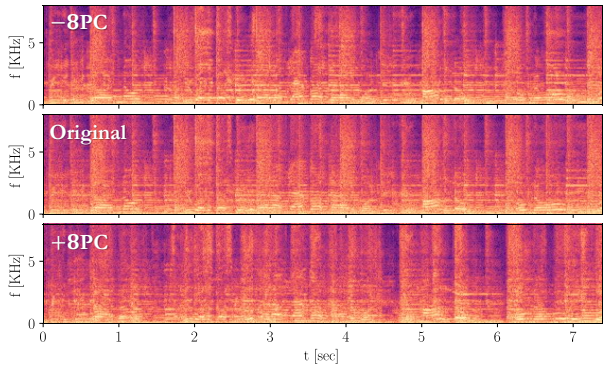

(c) Random directions, $\gamma = 8$.

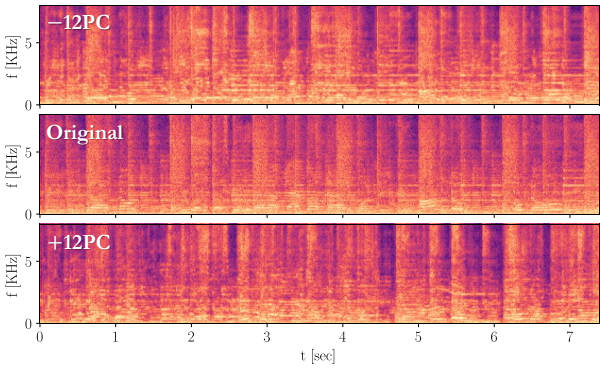

(d) Random directions, $\gamma = 12$.

Figure 14. **Our PCs vs. random directions.** While our method extract PCs with a clear semantic meaning (14a), *e.g.*, isolating a singer or a guitar in a given signal, the effect of using random directions (14b),(14c),(14d) varies from producing unnoticeable changes with small γ factor to degrading the signal when large γ values are used. This result can be listened to in Sec. 3 of our examples page. We fix $t' = 65$ for our method, and apply our or the random directions for $T_{\text{start}} = 200$, $T_{\text{end}} = 1$. Both samples were generated using the music checkpoint of AudioLDM2, with a source prompt randomly chosen from our prompts dataset.

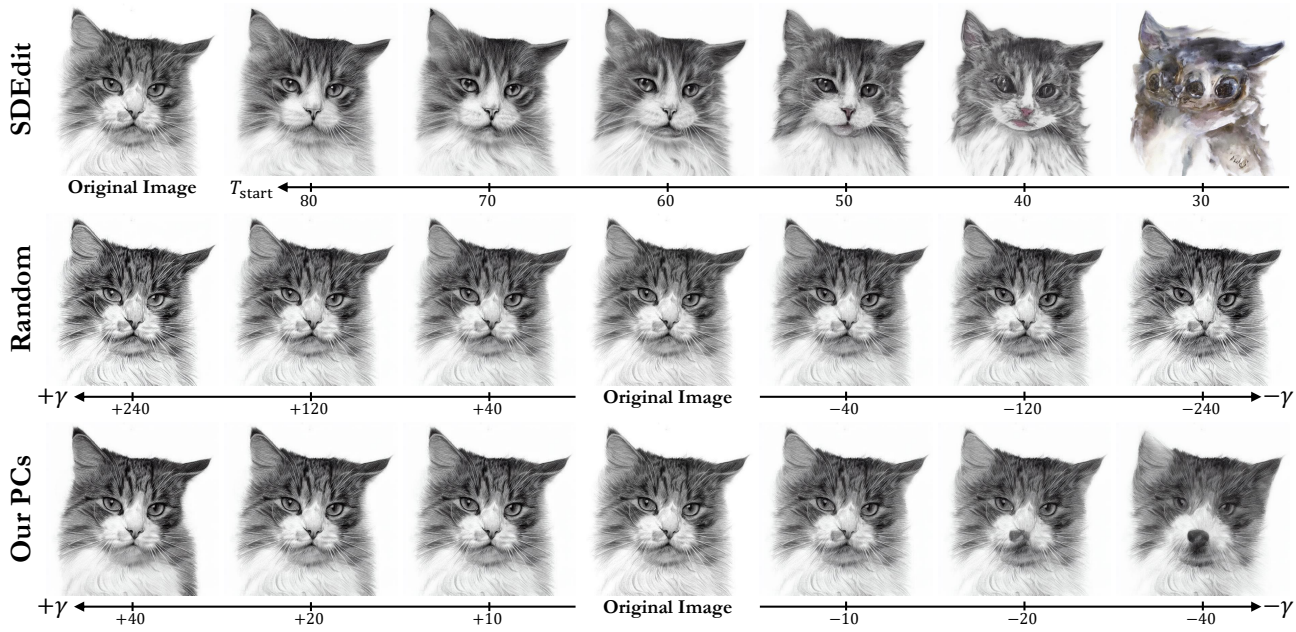

Figure 15. **Unsupervised zero-shot editing of images.** We demonstrate the applicability of our unsupervised approach for extract editing directions using Stable Diffusion (Rombach et al., 2022) on images taken from "modified ImageNet-R-TI2I" (Tumanyan et al., 2023), contrasted with SDEdit (Meng et al., 2021) and our previously proposed random baselines (See App. E. Our method extracts editing directions that carry a semantic meaning, *e.g.*, a direction for changing the species of the cat or making it a more distinct cat-breed, while retaining the original essence of the image.

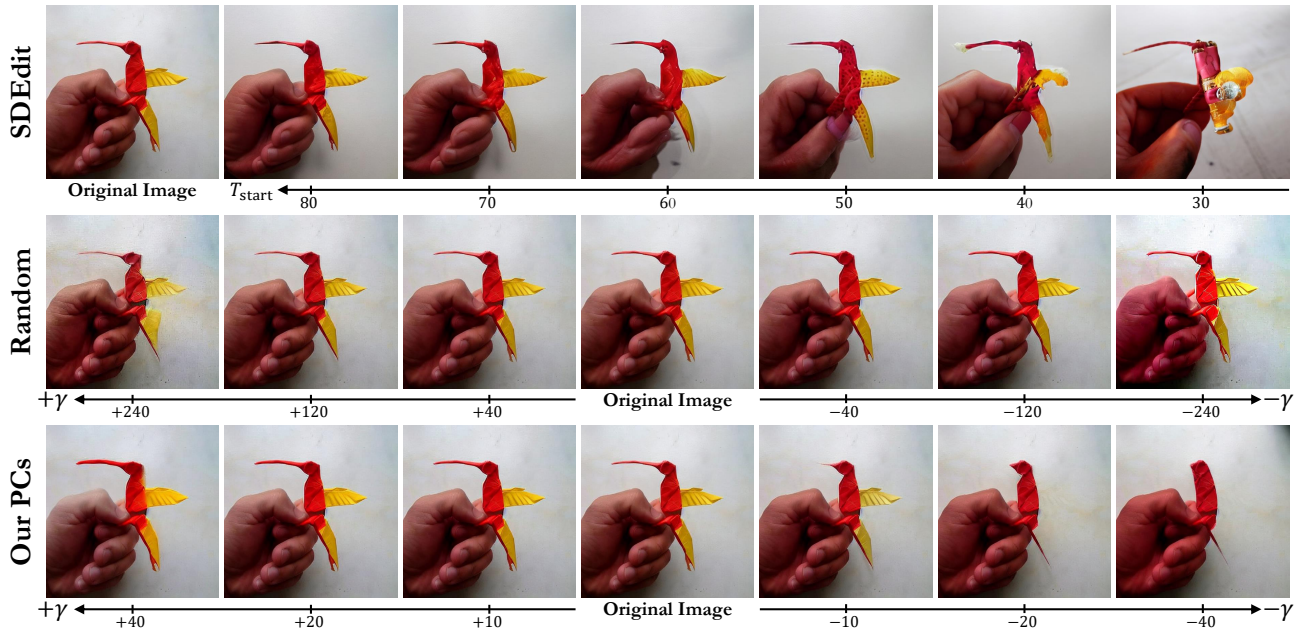

Figure 16. **Unsupervised zero-shot editing of images.** We demonstrate the applicability of our unsupervised approach for extract editing directions using Stable Diffusion (Rombach et al., 2022) on images taken from "modified ImageNet-R-TI2I" (Tumanyan et al., 2023), contrasted with SDEdit (Meng et al., 2021) and our previously proposed random baselines (See App. E. Our method extracts editing directions that carry a semantic meaning, *e.g.*, thickening the beak of a bird or shortening it until it is no longer a bird and the wings dissapear, while retaining the essence and structure of the image, *e.g.*, not degrading the hand.

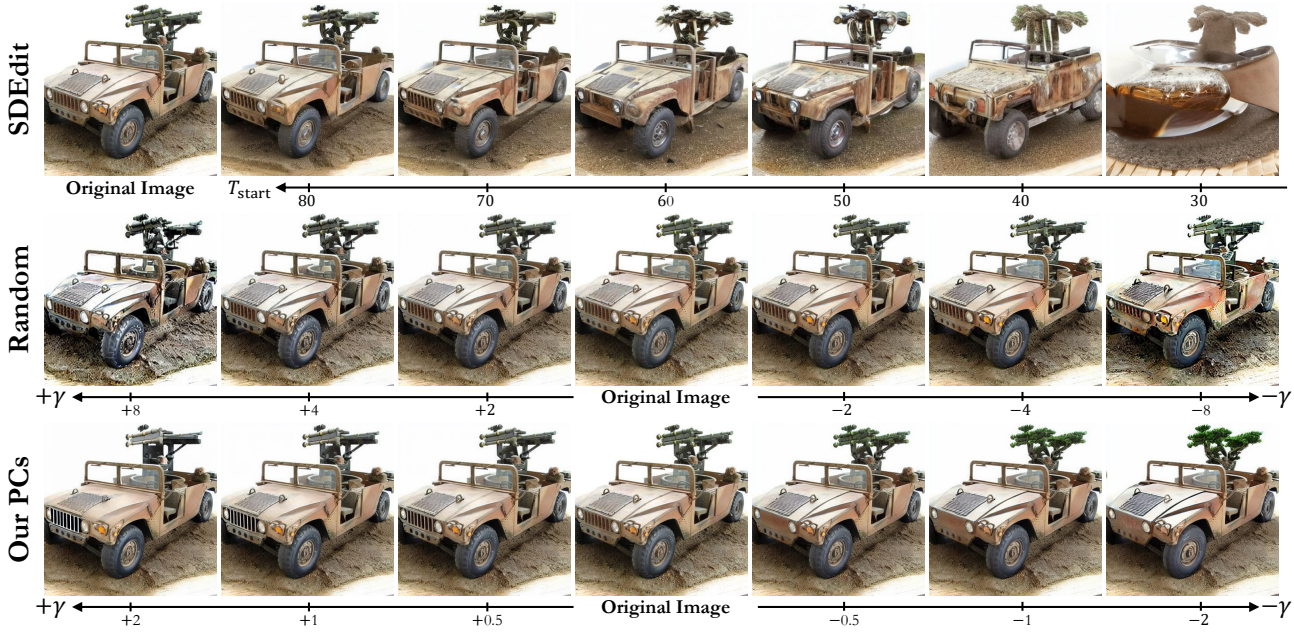

Figure 17. **Unsupervised zero-shot editing of images.** We demonstrate the applicability of our unsupervised approach for extract editing directions using Stable Diffusion (Rombach et al., 2022) on images taken from "modified ImageNet-R-TI2I" (Tumanyan et al., 2023), contrasted with SDEdit (Meng et al., 2021) and our previously proposed random baselines (See App. E. Our method extracts editing directions that carry a semantic meaning, *e.g.*, turning a gun to a bonsai tree, while retaining the essence and structure of the image, *e.g.*, keeping the jeep toy car relatively the same.